UNIVERSIDADE DE LISBOA
FACULDADE DE CIÊNCIAS
DEPARTAMENTO DE QUÍMICA E BIOQUÍMICA

Study of the self-assembly of the pro-inflammatory S100A9 protein driven by metal ion binding

Mestrado em Bioquímica
Especialização em Bioquímica

Gonçalo Raimundo Nogueira

Dissertação orientada por:
Professor Doutor Cláudio M. Gomes

2016

Acknowledgments

I would like to express my gratitude to Professor Cláudio M. Gomes, for welcoming me in his laboratory, for the learning opportunity and mentorship, for his support, patience, criticism and motivation.

A special thank you to my friends and colleagues at the Proteins Folding and Misfolding Lab:

To Joana Cristovão, Tânia Lucas, Bárbara Henriques and Sónia Leal, for their patience, constant ideas and guidance during my first steps as a scientist.
To thank Rodrigo David and Javier Fernandez for being the boys from the group and also Mariana Romão for their friendship inside and outside the lab.
Words cannot express how grateful I am for the good moments that we shared and for providing a happy and comfortable working environment.

I would like to thank Prof. Margarida Godinho, Prof. Mário Rodrigues and Dr. Carlos Marcuello from the BioISI Magnetic Nanosystems Group and FCUL Department of Physics for the AFM measurements and analysis.

Finalmente, quero agradecer à minha família, amigos e, em especial, à Nocas, pelo amor e apoio incondicional. A pessoa que sou hoje devo-o a vocês.

Abstract

S100A9 is a Ca^{2+} and Zn^{2+}-binding protein which has been increasingly associated with Alzheimer's disease due to its dual roles as a pro-inflammatory and amyloidogenic agent. This neurodegenerative condition is characterized by neuroinflammation, amyloidogenesis and also disturbance of metal homeostasis. Previous studies have shown that S100A9 is capable to undergo self-assembly into dimer, tetramer and larger oligomers, including formation of amyloid fibrils as a result of its inherent amyloidogenicity. Interestingly, the formation of these different conformational states is thought to be regulated by Ca^{2+} and Zn^{2+} binding. Herein, we provide insights of how binding of these metal ions influences S100A9 self-assembly reactions using a set of complementary techniques, including fluorescence spectroscopy with different conformational dyes, conformational antibodies, SEC analysis, turbidimetry assays, and AFM imaging.

The results obtained suggest that Zn^{2+} binding induces the formation of S100A9 assemblies and precipitates; albeit these exhibited ThT-reactivity, AFM imaging elicited mostly amorphous aggregates rather than amyloidogenic fibril structures. SEC analysis of the formed oligomers indicated a size corresponding to that of the S100A9 tetramer, a finding corroborated by AFM measurements. Regarding Ca^{2+}-binding effects, thioflavin-T (ThT)-binding kinetics indicate the occurrence if a polymerization reaction, which leads to the formations of string-like structures as noted by AFM. Interestingly, in control experiments using apo-S100A9, we observed that these string-like structures are also formed upon reaction in the same conditions with no added metal ions. When exposed to both Zn^{2+} and Ca^{2+}, we noted that S100A9 forms heterogeneous self-assemblies, as inferred from reactivity with different fluorophores including luminescent conjugated oligothiophene dyes which are able to detect a wide range of amyloidogenic protein aggregates. Interestingly, we observed that metal ion chelation using EDTA fully reverts the self-assembly reaction, as shown by disappearance of turbidity, decrease in ThT emission and a decrease on AFM-observable oligomers/structures.

Altogether, the results from this work contribute to unveil possible mechanisms through which Zn^{2+} and Ca^{2+} binding influences S100A9 self-assembly reaction and will open new avenues for investigations on the roles of such assemblies in pathophysiological conditions.

Keywords: S100A9, protein aggregation, protein self-assembly, metal ions

Resumo

A causa de doenças neurodegenerativas está muitas vezes associada à formação de agregados proteicos e estruturas amiloides. Um exemplo mais representativo desta situação é a doença de Alzheimer, que se caracteriza pela existência de um cenário de neuro-inflamação e amiloidogénese. Neste contexto biológico, ocorre a acumulação do péptido β-amiloide (Aβ) em placas extracelulares e a deposição da proteína tau na forma híper-fosforilada em emaranhados neurofibrilares intracelulares. Como consequência deste fenómeno, o principal sintoma da doença é a deterioração das capacidades cognitivas, porém, os mecanismos subjacentes a estes sintomas não são ainda totalmente compreendidos. Além disso, a desregulação da homeostase dos metais é também observada em pacientes que sofrem desta patologia.

A proteína S100A9 tem vindo a ser frequentemente associada com a doença de Alzheimer devido ao seu papel tanto como agente pro-inflamatório e amiloidogénico. A S100A9, também conhecida como Mrp14, pertence à grande família das proteínas S100, as quais possuem dois domínios *EF-hand* de ligação a cálcio (Ca^{2+}), ligando também zinco (Zn^{2+}) e cobre (Cu^{2+}) em locais distintos dos locais de ligação do Ca^{2+}. Esta proteína é uma das mais potentes proteínas pro-inflamatórias da família S100, sendo sobrexpressa em cenários inflamatórios, incluindo a inflamação decorrente na doença de Alzheimer. Estudos prévios demonstraram que a proteína S100A9 tem a capacidade de se reorganizar-se (*self-assembly*) em dímero, tetrâmero e também em estruturas oligoméricas maiores, onde se inclui a formação de fibras amiloides, como resultado da sua amiloidogenicidade inerente. Deste modo, sabendo que esta proteína tem a capacidade de ligar Ca^{2+} e Zn^{2+}, e que, por sua vez, a ligação dos metais a proteínas é um fenómeno que induz alterações conformacionais na estrutura das mesmas, foi proposto que a interacção entre a proteína S100A9 e os iões metálicos pode ser a causa da agregação amilóide e da citotoxidade que advem deste fenómeno. Assim, neste estudo são dadas evidências de como os metais influenciam a reacção de *self-assembly* da proteína S100A9, através do uso de técnicas complementares, nomeadamente espectroscopia de fluorescência recorrendo ao uso de diferentes sondas conformacionais (ThT, ANS, LCOs: p-FTAA e h-FTAA), ensaios de turbidimetria, uso de anticorpos conformacionais (OC e A11), analise por cromatografia de exclusão molecular e também microscopia de força atómica (AFM).

Numa primeira parte deste estudo, foi necessário expressar e purificar o homodímero da proteína S100A9 de modo a serem obtidas quantidades significantes de proteína pura, para que os subsequentes ensaios pudessem ser efectuados. Para tal, a proteína recombinante humana foi expressa em *E.coli,* seguindo-se uma sequência de etapas, que permitiram isolar os corpos de inclusão e extrair as proteínas contidas nestes, incluindo a proteína em estudo. O extracto proteico foi após submetido a uma serie cromatografias: cromatografia de dessalinização, para remover o cloreto de guanidina (agente desnaturante), cromatografia de exclusão molecular e cromatografia de troca-iónica. Finalmente, e dado que o principal objectivo deste estudo era avaliar o efeito dos iões metálicos (Ca^{2+} e Zn^{2+}) na proteína S100A9, foi necessário desmetalar a proteína pura obtida. Para tal, o extracto foi incubado com DTT e EDTA, seguindo-se nova cromatografia de exclusão molecular, de modo a obter a forma pura final da proteína desmetalada.

Neste estudo, demonstramos que o Zn^{2+} tem a capacidade de induzir a agregação da proteína S100A9, quando presente em concentrações superiores à capacidade da sua ligação à proteína S100A9 e quando esta última está presente numa concentração superior a 10μM (concentração critica para agregar). Os agregados formados apresentaram reactividade para com a sonda ThT (usada para detetar estruturas amiloides) e foram visíveis, macroscopicamente, sob a forma de um precipitado branco, conferindo um aspecto turvo, que possibilitou seguimento

deste fenómeno por ensaios onde monitorizou a turbidez da solução a 360 nm. A formação deste precipitado ocorreu numa escala de tempo de minutos. Além disso, observou-se que o aumento da quantidade de Zn^{2+} se correlacionou com um potenciamento do processo de agregação, onde se observou um aumento do sinal em ambos os ensaios (fluorescência e turbidez) e diminuição da fase de inicial (*lag phase*). Os resultados com as outras sondas conformacionais mostraram estar de acordo com a existência desta agregação. No entanto, apesar de os agregados formados levarem à formação de espécies reactivas à ThT e aos LCOs, os resultados obtidos através de ensaios de *seeding*, análise por AFM e detecção com os anticorpos conformacionais, OC e A11, sugerem que os agregados formados não são de origem amilóide, mas por outro lado que parecem ser maioritariamente de natureza amorfa. A divergência de resultados pode ser devida ao facto da sonda ThT ter já ter mostrado capacidade de se ligar não só a estruturas amiloides mas também de outra natureza. A possibilidade de estes agregados serem induzidos por interações electrostáticas que afectam a solubilidade da proteína foi excluída, uma vez que as cinéticas de S100A9 em presença de excesso de NaCl não conseguiram reproduzir o mesmo efeito que o Zn^{2+}. Por último, a análise das amostras de S100A9 incubadas com Zn^{2+} (razão 4:1), por cromatografia de exclusão molecular, foi possível observar a presença de espécies com um tamanho semelhante ao da proteína S100A9 na sua forma tetramérica, o que está concordante com o ensaio de AFM. Estes resultados sugerem que o Zn^{2+} induz a formação de agregados não amiloides, que precipitam, com um possível papel na quelação do Zn^{2+}.

Relativamente ao efeito do Ca^{2+}, sendo este um ligando natural da proteína S100A9, seria expectável que a ligação deste ião metálico não induzisse a agregação amilóide da proteína. De facto, os ensaios de cinética de ligação das várias sondas conformacionais e de imunodetecção pelos anticorpos OC e A11, excluíram a existência de formação de estruturas amiloides. Em concordância, as imagens obtidas por AFM indicam a ocorrência de uma reacção de polimerização do tipo não-amilóide, onde a proteina S100A9 adquire uma aparência semelhante longas "cordas". Curiosamente, um ensaio controlo usando a forma apo da proteína S100A9, revelou a formação de estruturas semelhantes, mesmo sem a adição de iões metálicos. Estas evidências sugerem uma possível função biológica destes agregados.

Curiosamente, quando combinada a ligação de Zn^{2+} e Ca^{2+} à S100A9 observou-se um efeito aditivo que se refletiu numa agregação heterogénea, com presença de fibras amiloides e outros agregados intermediários passiveis de serem observados por AFM e de serem detectados pelos anticorpos conformacionais OC e A11. Além disso, todas as sondas mostram reactividade para com a S100A9, mas de uma forma sequenciada, demostrando a complexidade deste fenómeno. Neste caso, à semelhança da agregação induzida apenas pelo Zn^{2+}, a solução tornou-se túrbida com formação de precipitado branco.

Por fim, é de salientar que foram efectuados ensaios com EDTA, um agente quelante, para remover os iões metálicos ligados à S100A9 com o objectivo de verificar a dependência dos agregados formados. Assim, foi observada a reversão da reacção de *self-assembly* pelo desaparecimento da turbidez, diminuição da fluorescência da ThT e diminuição dos oligómeros/estruturas observadas por AFM.

Em suma, este estudo contribuiu para revelar possíveis mecanismos, pelos quais a ligação de Zn^{2+} e/ou Ca^{2+} à proteína S100A9 influencia a sua reacção de *self-assembly*. Abrindo, assim, caminho para investigação dos papéis dos vários agregados em condições patológicas, nomeadamente na doença de Alzheimer, e para evidenciar o papel e a relevância da proteína S100A9 no despoletar da doença.

Palavras-chave: S100A9, agregação proteica, iões metálicos, enrolamento de proteínas

Contents

List of Figures

List of Tables

Abbreviations

°C	Celsius degrees
µmol	Micro mole
Abs280	Absorbance at 280nm
AD	Alzheimer's disease
AFM	Atomic Force Microscopy
ANS	8-anilino-1-naphthalenesulfonic acid
Asn	Asparagine
Asp	Aspartic Acid
Aβ	amyloid-β protein
Ca	Calcium
Cu	Copper
Cys	Cysteine
DNA	Deoxyribonucleic acid
DTT	Dithiothreitol
E. Coli	*Escherichia coli*
EDTA	ethylenediaminetetraacetic acid
EGTA	Triethylene glycol diamine tetraacetic acid
ER	Endoplasmic Reticulum
Fe	Iron
G	Free energy
g	Gram
Gln	Glutamine
Glu	Glutamic Acid
H	Enthalpy
h	Hour
His	Histidine
Hsp	Heat Shock Protein
IPTG	Isopropyl β-D-1-thiogalactopyranoside
kDA	Kilo Dalton
L	Litre
LCOs	luminescent conjugated oligothiophenes
M	Molar
min	Minutes
mL	Mili liters
mM	mili Molar
mAu	milli Absorbance Unit
N	Nitrogen
NaCl	Sodium Chloride
nm	Nanometers
nmol	Nano mole
OD600	Optical density at 600 nm
PAGE	Polyacrylamide gel electrophoresis
PDB	Protein Data Bank
Phe	Phenylalanine
pI	Isoelectric point

PMSF	phenylmethane sulfonyl fluoride
s	second
SDS	sodium dodecyl sulfate
SEC	Size-exclusion chromatography
TCEP	tris(2-carboxyethyl)phosphine
ThT	Thioflavin-T
TLR	Toll Like Receptor
Trp	Tryptophan
Tyr	Tyrosine
µM	micro Molar
Zn	Zinc

I. Introduction

1.1. Protein Folding and Misfolding

1.1.1. Protein folding

Proteins are essential in a variety of biological functions and, to work properly, following their synthesis on the ribosome, they must undergo through a complex process named folding. This process consists on the acquisition of a specific three-dimensional structure, native conformational state, which is encoded in each protein's own amino acid sequence [1, 2].

Uncovering protein folding pathways and the principles underlying this phenomenon is considered to be one of the most challenging problems in all structural biology [1-3]. Protein folding is a high efficiency and tightly regulated physical process that originates a wide range of defined structures which vastly contributed for biological living systems to develop diversity and selectivity in their biochemical processes [3].

Indeed, only the proteins that have folded correctly will acquire long-term stability in crowded biological environments and will be able to selectively interact with their natural partners. Consistently, unsuccessful protein folding is frequently associated with pathological scenarios [2-6].

The folding mechanism results from a set of interactions formed between a specific group of amino acid residues that comprises de core of the folding which in turn triggers the folding reaction, into the final conformation [7]. The latter corresponds to the so-called native state, which tends to be the most stable structure under physiological conditions [8].

Proteins are structurally organized in a hierarchical manner. The first level of this hierarchy is the primary structure, which correspond to the sequence of amino acids that composes the protein chain. Within this chain, certain segments tend to fold into simple shapes, such as helices and loops, etc, that together constitute the secondary structure. The overall chain tends to fold further into a three-dimensional compact tertiary structure, the most stable form of the protein, since it optimizes the various attraction forces between the different amino acids residues. Moreover, the tertiary structure correspond to active form of the protein, thus it is often referred to as the native structure of the protein. These levels of structure exist in all proteins, although sometimes deviations from the classical "rules" occur, namely in the formation of fibrous proteins [9]. Some proteins are composed of more than one chain, in which cases the tertiary structure is not the final hierarchical level of structure. In these cases, each chain must fold separately into a tertiary structure and then join together to form a biologically active complex, referred to as quaternary structure [9].

In order to achieve the native state, proteins have to find their way to this unique conformation rather than one of the countless alternatives. Preferable folding pathways are determined by the folding landscape of protein which can be conceptually described as a funnel [10]. This concept allows the correlation between free energy changes and the protein's three-dimensional structure (Figure 1.1.1) [7]. The top of the funnel contains a wide variety of unfolded conformations characterized by high energy levels resulting from a large conformational entropy [10]. Contrarily, the bottom of the funnel presents an energetic minimum corresponding to the most stable structure under physiological conditions [10].

The energetics of protein folding can be described by the central thermodynamic equation (equation 1):

$$\Delta G = \Delta H - T\Delta S \qquad \text{(Equation 1.1.1)}$$

In this equation, ΔH represents the additive contributions of chemical bonds and interactions, while $-T\Delta S$ correspond to the variations in the degree of order within the system [8].

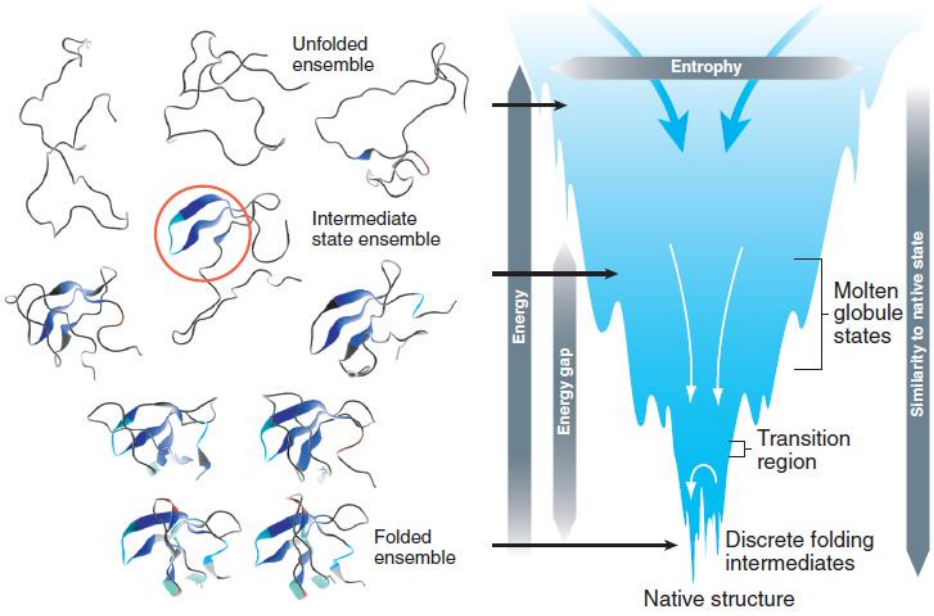

Figure 1.1.1 – The free energy landscape for protein folding. Folding occurs through the progressive organization of ensembles of structures on a funnel-shaped free energy landscape. Conformational entropy loss during folding is compensated by the free energy gained as more native interactions are formed. Kinetics is determined by the local roughness of the landscape, relative to thermal energy. Adapted from [10].

Folding in vivo can occur in different occasions and cellular locations. On the one hand, it can happen co-translationally, when the nascent chain is still attached to the ribosome [11]. On the other hand, in most case protein folding occurs in the cytoplasm after translation. Additionally, folding can take place in subcellular compartments, such as the mitochondria or the endoplasmic reticulum (ER), after the translocation of the polypeptide chain through the organelle membrane occurs [12, 13]. The particular environment in which folding takes place makes a difference in many details, however the fundamental principles of folding are indeed universal [3].

1.1.2. Protein folding regulation

Considering the above-mentioned complexity of the protein folding process, misfolding events can happen, therefore leading to unsuitable interactions with other molecules inside of the cell [14]. As such, living systems have strategically evolved to prevent such phenomena [12-14]. The folding process takes place in a complex and highly crowded environment, where it is aided by auxiliary proteins, termed molecular chaperones, whose role is to secure the protein's proper folding [12-16]. Chaperones act both in an early stage of protein synthesis, interacting with the chain as it emerges from the ribosome, and also at later stages, guiding the protein folding after the dissociation from the ribosome [12, 13].

The role of molecular chaperones in protein folding is to increase the efficiency of the overall process by reducing the probability of competing reactions, particularly misfolding and ultimately aggregation. Thus it is often observed the tandem work of different molecular chaperones to guarantee the success of the various stages of the protein folding [3].

One of main classes of molecular chaperones are the heat shock proteins (Hsps). Hsps are especially induced in conditions of cell stress, which is consistent with their role in preventing misfolding. Hsps are classified according to their molecular weight (Hsp40, Hsp60, Hsp70, Hsp90, Hsp100…) and are involved not only in protecting proteins as they fold but also in rescuing misfolded and even aggregated proteins, allowing them to fold correctly [12, 13].

Potentially slow steps in the folding process can be accelerated by a group proteins that act as folding catalysts, such as peptidylprolyl isomerases and protein disulphide isomerases. Their role is to increase the rate of the cis–trans isomerization of peptide bonds comprised in proline residues, and to increase the rate of formation and reorganization of disulphide bonds, respectively [17].

As mentioned above, folding can take place in different cellular locations. In this context, newly synthesized proteins, meant for secretion, are translocated to the ER, where the folding process happens. In the ER, proteins are subjected to a "quality-control" check that involves a series of glycosylation and deglycosylation reactions that tags proteins, allowing the distinction between the correctly folded from misfolded ones (Figure 1.1.2) [18, 19]. Misfolded proteins are targeted for degradation [20]. This mechanism is also upregulated in stress conditions [21].

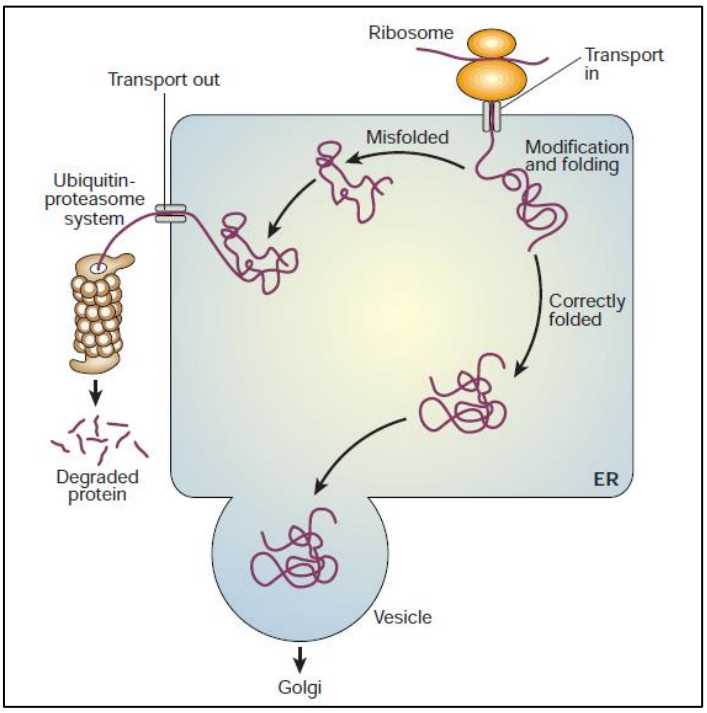

Figure 1.1.2 - Regulation of protein folding in the ER. Many newly synthesized proteins are translocated into the ER, where they fold into their three-dimensional structures with the help of a series of molecular chaperones and folding catalysts (not shown). Correctly folded proteins are then transported to the Golgi complex and then delivered to the extracellular environment. However, incorrectly folded proteins are detected by a quality-control mechanism and sent along another pathway in which they are ubiquitinated and then degraded in the cytoplasm by proteasomes. Adapted from [19].

1.1.3. Metal ions and protein folding

Metal ions are essential for virtually all organisms and metal-binding proteins constitute around one third of the proteome [8]. Among others, metal cations such as iron (Fe^{3+}/Fe^{2+}), zinc (Zn^{2+}), copper (Cu^{2+}/Cu^{+}), calcium (Ca2+), magnesium (Mg2+) or manganese (Mn^{2+}/Mn^{3+}) are extremely important in biological processes such as electron transfer reactions, catalysis and stabilization of the protein structure [22]. The protein-metal association leads to a series of adjustments on the protein fold that results from a compromise on coordination numbers, bond lengths and angles which are imposed both on the metal and on the protein fold [8]. These changes alter protein energetics, thus influencing its stability and dynamic properties [22]. There are amino acid residues, such as histidine, cysteine, aspartate and glutamate, that have high affinity to certain metals resulting in a selectivity pattern [22-24]. Hence, there are preferable combinations of amino acids residues, which constitute metal coordination motifs, whose interaction with the metal ion ensures its proper insertion in a catalytic or structural site (Table 1.1.1) [8].

Table 1.1.1 – Typical coordination environments of selected metal cations in proteins. Adapted from [8].

Metal cation	Bond stability	Coordination number	Side chain ligands	Coordination geometry
Zn^{2+}	High	3	His, Cys, Glu	Severely distorted tetrahedron
Cu^{+}	High	3,4	His, Cys, Met	Severely distorted tetrahedron
Cu^{2+}	High	3,4	His, Cys	Distorted square planar
Ca^{2+}	Intermediate	7 (8)	Glu, Asp	Pentagonal bipyramid, trigonal prism, distorted octahedron
Fe^{2+}	Low	4–6	His, Glu, Asp Cys	Distorted octahedron tetrahedron
Fe^{3+}	High	4–6	Glu, Asp, Tyr Cys	Distorted octahedron tetrahedron

Generally, the protein-metal association involves both electrostatic and coordinative interactions, but in around one third of metalloproteins metal binding is essentially coordinative [8, 24]. Alternatively, this interaction can be established indirectly via a metal cluster or a larger chemical group [8].

When multiple binding sites are involved, the protein fold energetics become more complex due to cooperative events. In this cases, when a metal binds or dissociates from one site, conformational adjustments occur that affects the coordination sphere and binding energetics of another site, either by increasing (positive cooperativity) or decreasing (negative cooperativity) its affinity [8].

It is now clear that metal binding modulates both the protein folding landscape and folding trajectories [25, 26]. Thus, living systems have created a complex protein machinery whose function is the maintenance of metal ion homeostasis [8]. The metal delivery to polypeptides is assured by metallo-chaperones, whose role is to deliver the metal ion to its target hollo protein [27]. There are three generic scenarios of the mechanisms that mediate metal insertion into newly folded proteins: co-translational metal ion binding; post-translational metal ion binding to incompletely folded proteins; and post-translational metal ion binding to folded apo proteins [24].

1.1.4. Protein aggregation and amyloid formation

In addition to the native globular structure, proteins can populate other states, including disordered and partially ordered conformations, and different aggregated assemblies, which are important to cell homeostasis including growth, development and proliferation (Figure 1.1.3) [3]. The state a protein adopts under specific conditions depends on the relative thermodynamic stabilities of the many accessible conformations and on the kinetics of their interconversion (Figure 1.1.3) [2, 28]. The transitions between the different states are highly regulated by the environment and by the presence of molecular chaperones and degradation mechanisms. Therefore, aberrant behavior of the chaperones and other intervenients can be a key factor for development of misfolding and aggregation diseases (Table 1.1.2) [21, 29].

Table 1.1.2 – Representative protein folding diseases. Adapted from [2].

Disease	Protein	Site of folding
Hypercholesterolemia	low-density lipoprotein receptor	ER
Cystic fibrosis	Cystic fibrosis trans-membrane regulator	ER
Phenylketonuria	Phenylalanine	cytosol
Huntington's disease	Huntingtin	cytosol
Marfan syndrome	Fibrillin	ER
Osteogenesis imperfecta	procollagen	ER
Sickle cell anaemia	hemoglobin	cytosol
αl-antitrypsin deficiency	αl-antitrypsin	ER
Tay-Sachs disease	β -hexosaminidase	ER
Scurvy	Collagen	ER
Alzheimer's disease	β-amyloid/presenilin	ER
Parkinson's disease	α-synuclein	cytosol
Scrapie/Creutzfeldt-Jakob disease	prion protein	ER
Familial amyloidoses	transthyretin/lysozyme	ER
Retinitis	pigmentosa rhodopsin	ER
Cataracts	crystallins	cytosol
Cancer	p53	cytosol

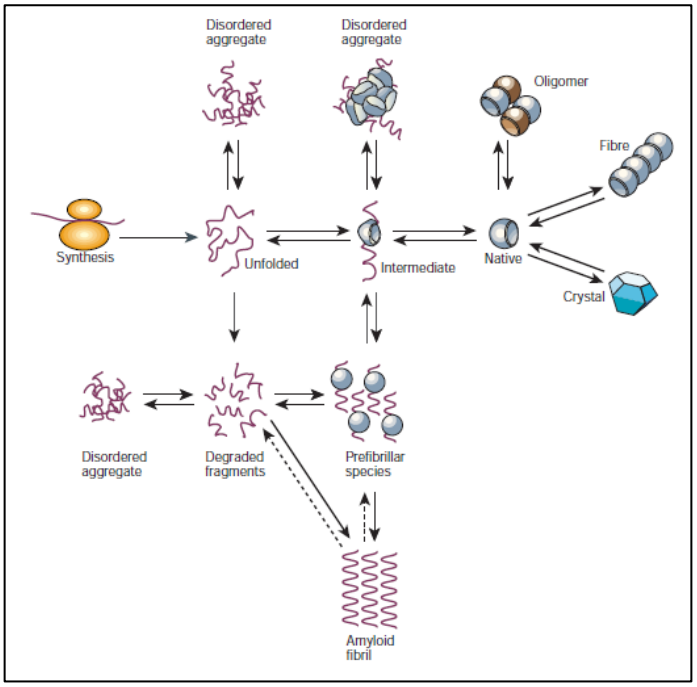

Figure 1.1.3 – States accessible to a protein molecule. Adapted from [28].

Amyloid fibrils are the most well studied type of protein aggregate, given its unique kinetic and thermodynamic stability that culminates a progressive build-up of deposits in tissues. As a consequence, these deposits can physically disrupt specific biological components such as organs and tissues, thereby leading to a pathological behavior [5].

Several peptides and proteins that are involved in the most common misfolding diseases, such as the amyloid-β peptide in Alzheimer's disease [30, 31] and α-synuclein in Parkinson's disease [32, 33], form amyloid fibrils. Although their soluble forms have distinct characteristics, the aggregated forms are typically similar, characterized by their cross-b structure, in which β-strands form effectively continuous hydrogen-bonded β-sheets that run along the length of the fibril [34, 35]. Amyloid fibrils tend to appear as unbranched filamentous structures with a few nanometers in diameter but often micrometers in length (Figure 1.1.4) [36].

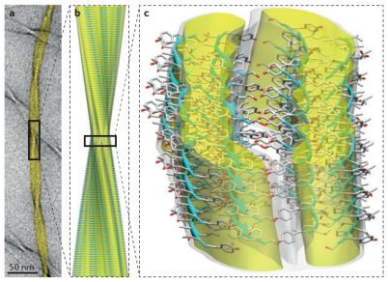

Figure 1.1.4 - Structure of an amyloid fibril at atomic resolution. Adapted from [36].

This phenomenon is not restricted to a small number of proteins, but instead it seems to be a generic feature of polypeptide chains, since it has been shown that fibrils can be formed *in vitro* by many other peptides and proteins, under specific conditions [2, 37, 38]. However, the propensity to form amyloid fibrils under given circumstances can differ between different amino acid sequences. The amyloidogenic propensity of a given peptide or protein correlates with its physicochemical features, such as charge, secondary-structure propensities and hydrophobicity [39].

The highly ordered and compact structure, provides an exceptional high level of kinetic and thermodynamic stability to the fibrils, which led to the assumption that the amyloid state might be more stable than the functional native state of a protein, even under physiological conditions [40, 41]. However, in the amyloid state intramolecular interactions are predominant and essential, which means that its thermodynamic stability (ΔG) is dependent on the protein concentration [42]. Thus, the amyloid state in only more stable than the native state when the critical concentration is achieved and the free energy (G) of the peptide or protein is lower than its native state. This evidence suggests that proteins might occasionally function at concentrations that exceed their conventional thermodynamic solubility [41, 43].

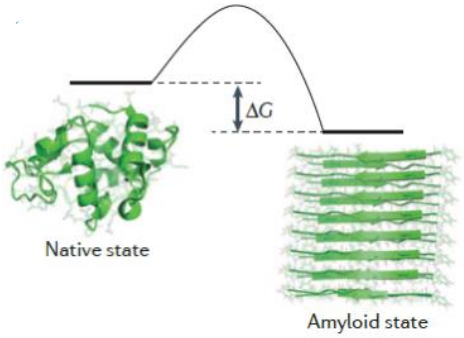

Figure 1.1.5 – Thermodynamics of the amyloid state. Adapted from [40].

The formation of amyloid fibrils has been characterized, by in vitro studies, as a typical nucleated process composed by a lag phase, followed by a period of rapid growth [44, 45] and if the total amount of protein is limited, this process ends with a plateau phase as a result of the depletion of all soluble species and its conversion into fibrils (Figure 1.1.7). The self-assembly into amyloid fibrils begins with the formation of soluble oligomers resulting from nonspecific interactions, however, in some cases, specific structural transitions are a key factor [46]. The earliest species generally are characterized as small bead-like structures, sometimes linked together, often described as amorphous aggregates or micelles. Sequentially, the "prefibrillar aggregates" give rise to short, thin and sometimes curly fibrillary species termed "protofilaments" or "protofibrils". Finally, the latter species are thought to assemble into long mature fibrils (Figure 1.1.6) [3].

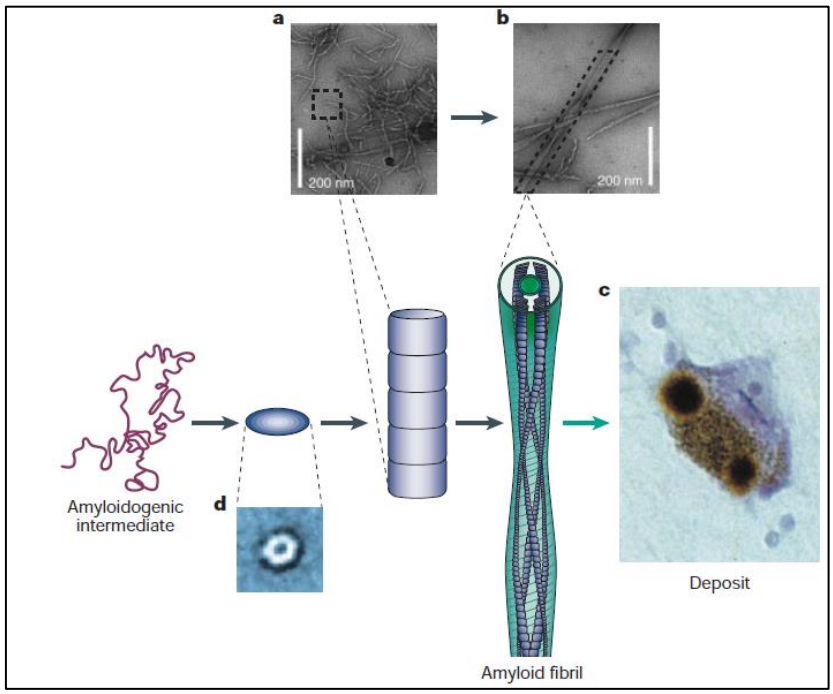

Figure 1.1.6 – General mechanism of aggregation to form amyloid fibrils. The earliest species generally resemble bead-like structures (D), thereafter transform into structures called protofibrils or protofilaments (A) which in turn assemble into mature fibrils (B). Adapted from [3].

Besides classic nucleation, the amyloid formation can be triggered by templating or seeding [47, 48] from existing aggregates. Templating is the mechanism by which structured aggregates promote the conversion of soluble protein species into similar aggregates [42]. On the other hand, the seeding process occurs when aggregates are used to promote the formation of larger aggregates, eliminating the lag phase [42].

The nucleation process can also involve secondary steps that depend on the behavior of the aggregates being formed [49, 50] (Figure 1.1.7). In this cases, formation of new aggregates arises from existing fibrils through fragmentation or from a combination of both monomeric and aggregated species through secondary nucleation [49, 50].

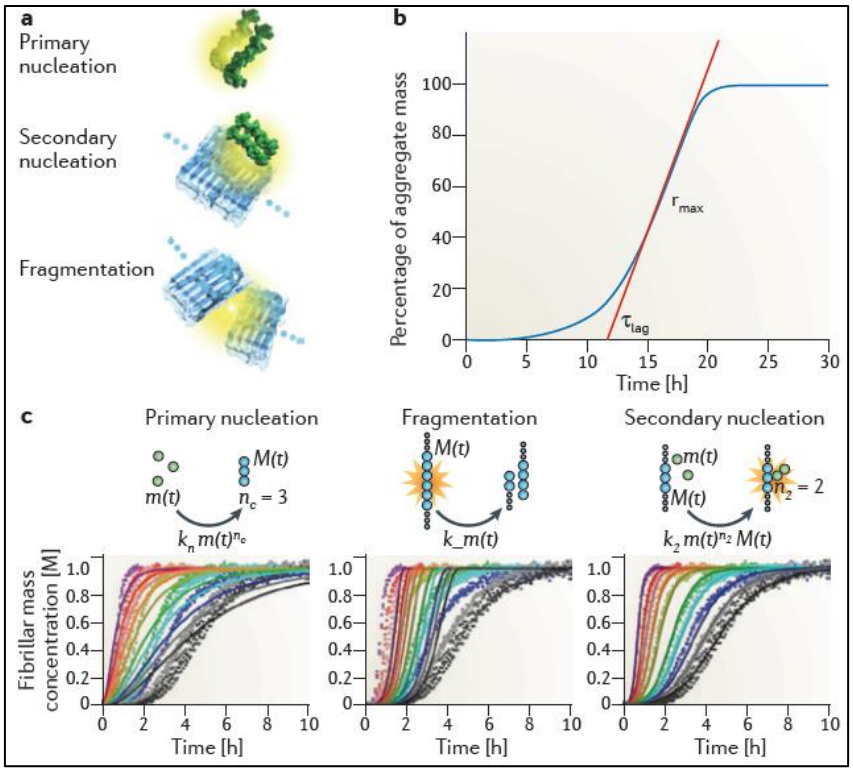

Figure 1.1.7 - Kinetics of amyloid formation. Adapted from [42]

The formation of these fibrils is known to be associated with both protein loss of function and generation of toxic intermediates in the process of self-assembly, which in turn are the basis of many misfolding diseases [30, 31, 49, 51-57]. Thus, living systems have evolved to avoid the formation of such fibrils by alternating amino acid residues with polar and hydrophobic characteristics [58, 59] that favor b-sheet structure seen in amyloid fibrils or by inserting highly aggregation-resistant residues, known as “gatekeepers” [58, 60], and by controlling proteins structure by means of molecular chaperones and degradation mechanisms [61-63].

1.2. S100 proteins

1.2.1. Function and structural characteristics of S100 proteins

S100 proteins belong to the EF-hand calcium-binding protein superfamily constituted by 24 members of low molecular weight (10–13 kDa) [64]. These proteins were named S100 by Moore, due to their solubility in 100% saturated ammonium sulfate [65].

Importantly, S100 proteins are expressed exclusively in vertebrates, exhibit tissue, cell, and subcellular-specific expression patterns [64, 66], and are induced by specific growth factors, cytokines and toll-like receptor (TLR) ligands [67-72]. In pathological conditions, however, the expression of a particular S100 protein can be triggered in a cell type that does not express it in normal physiological conditions [73-78]. The majority of the human S100 genes, are located within chromosome 1q21, except S100A11P, S100B, S100G, S100P and S100Z which map to chromosome 7q22-q3, 21q22, Xp22, 4p16 and 5q13, respectively [64].

All S100 proteins possess highly conserved overall structural architectures, although their sequences share no more than 25–65% homology [79]. Like other EF-hand Ca^{2+} binding proteins, the S100 proteins contain two calcium-binding EF-hand motifs bridged by a so called hinge region, that are highly conserved among the S100 family members (Figure 1.2.1) [80, 81]. A single monomer is composed of two calcium-binding helix-loop-helix motifs, containing four helices (helix I, II, III, and IV) (Figure 1.2.3) [80, 81].

These proteins are distinguished from other EF-hand proteins by their both intracellular and extracellular functions, their tendency to form homodimers, and the ability to bind transition metals at the dimer interface [82]. Some members of the S100 protein family are also able to form heterodimers, for example S100A8 and S100A9 or S100A1 and S100P, suggesting different functions for homo- and heterodimers [82]. Moreover, in many situations, biological functions and signalling are carried out by S100 proteins that form higher order non-covalent oligomers, which can be promoted through binding of metal ions, such as Ca^{2+} and transition metals (particularly Zn^{2+}) [82, 83]. These oligomers include tetramers (S100B [84] , S100A2 [85], and S100A8/A9 [86]), hexamers (S100B [84], S100A12 [87, 88]), and octamers (S100B [84]).

Regarding intracellular functions, S100 proteins are involved in the regulation of several biological processes such as proliferation, differentiation, apoptosis, Ca^{2+} homeostasis, energy metabolism, inflammation and migration/invasion, through the interaction with a variety of targets, namely enzymes, receptors, transcription factors and nucleic acids [89]. On the other hand, at extracellular level, S100 can regulate functions of target cells in an autocrine and paracrine manner via activation of surface receptors [89].

It has been shown that several S100 proteins have the ability to undergo β-aggregation, as a cause or consequence of pathophysiological states [90]. Indeed, an example is the S100A8/A9 heterodimer that was found in amyloid deposits from prostate cancer patients, in inclusions called *copora amylacea* [91]. Moreover, there is the assumption that S100 proteins have intrinsic disordered regions [92] and the propensity to form amyloid-like structures [91].

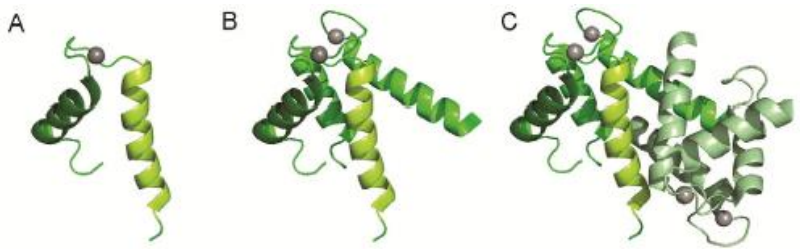

Figure 1.2.1 – Structural features of S100 proteins. Ribbon diagrams of (A) and EF-hand motif (B) and EF-hand domain and (C) the integration of two EF-hand domains into a S100A9 dimer. Adapted from [82].

1.2.2. Metal binding to S100

The ability of the S100 proteins to bind different metals, such as Ca^{2+}, Zn^{2+} and Cu^{2+}, is a matter of great interest since it is known that these metals can have an effect on the structure, function and biochemical properties of the protein [82]. Both Ca^{2+} and transition metals (particularly Zn^{2+}) have been shown to stimulate oligomerization in vitro, and crystal structures have revealed a range of oligomeric states [82].

As mentioned above, the S100 proteins bind Ca^{2+} ions through their EF-hand domains [80, 81]. Typically, EF-hand Ca^{2+}-binding motifs are arranged in pairs of EF-hands held together by a very short anti-parallel β-strand and numerous hydrophobic interactions between the four helices [82]. S100 family members are an unique set of EF-hand family, because one of the EF-hand motifs in the pair (designated as a pseudo- or S100-hand) has 14, rather than 12 residues (canonical EF-hand [93]), characterized by the lower affinity towards Ca^{2+} [94]. Each monomer is comprised of a S100-specific N-terminal EF-hand with a 14-residue Ca^{2+} binding loop, and a C-terminal EF-hand with a canonical 12-residue Ca^{2+} binding loop [80]. Since the proteins are dimers, each protein bind four Ca^{2+} ions, however, there are different affinities for this metal [82].

Similar to other EF-hand proteins, the S100 response to Ca^{2+} signals is characterized by conformational changes upon ion binding, which involves a significant shift in the orientation of Helix III, a 90 degree rotation (Figure 1.2.2) [95]. Moreover, this Ca^{2+}-induced conformational change leads to the exposure of a hydrophobic region necessary for the interaction with its specific protein targets. The hydrophobic region is composed by residues from the "hinge" section, Helix III and C-terminal, being the region with highest variability within the S100 family members [95-97].

As abovementioned, despite being structurally similar, S100 proteins are able to interact with a plethora of cellular targets. This characteristic diversity is secured by the fine tuning within the target binding site of each S100 protein, specific expression patterns and the metal-binding ability [98].

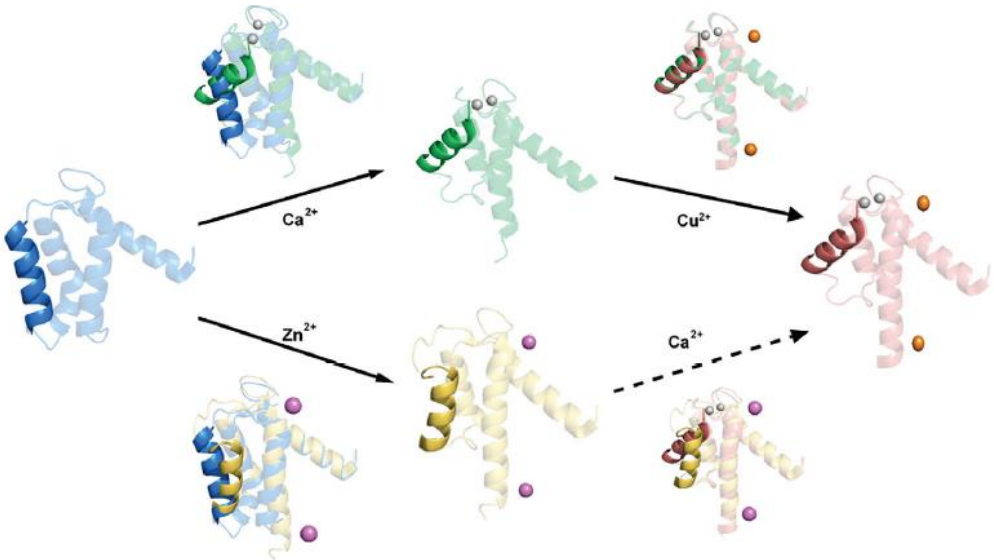

Figure 1.2.2 – Comparison of single sub-units of S100A12 to emphasize the differences in the packing of Helix III induced by Ca2+ and transition metals. This reveals that the consequences of binding Ca2+ are much greater than those of binding transition metals. Adapted from [82].

Interestingly, S100 proteins bind not only Ca^{2+} but also transition metals, such as zinc and copper, in other sites [99]. Indeed, the binding of Zn^{2+} to an S100 protein was firstly reported for the S100B protein [100]. However, it is now known that Zn binding occurs in several S100 proteins (S100A1, S100A2, S100A3, S100A5, S100A6, S100A7, S100A8/A9, S100A12, S100A16 and S100B), with high affinity ranging from *K*d=4 nmol L−1 (S100A3) to 100 μmol L−1 (S100A7). The Zn^{2+} binding S100 proteins can be classified into two categories: His-rich and Cys-rich [82].

Different studies [82] have revealed a conserved binding motif for the proteins with His-rich sites, composed by 4 His residues, or 3 His and 1 Asp residues, located at the dimer interface (Figure 1.2.3). Since the proteins are dimers, each protein binds two Zn^{2+} at the two symmetrically disposed sites (Figure 1.2.4).

For the S100A7 and S100A12 it has been shown, through a detailed comparative structural analysis between all states (apo form, Ca^{2+}- and Zn^{2+}-loaded), that in the Zn^{2+}-loaded structures of S100A7 and S100A12, two Zn^{2+} ions are bound at the symmetrically disposed sites (Figure 1.2.4 A), coordinated by three His N2 atoms (His17, His86, His90) and an aspartate side chain (Asp24) (Figure 1.2.4 A) [99, 101]. In all cases, the primary effect of Zn^{2+} is to alter the orientation of Helix III (Figure 1.1.2).

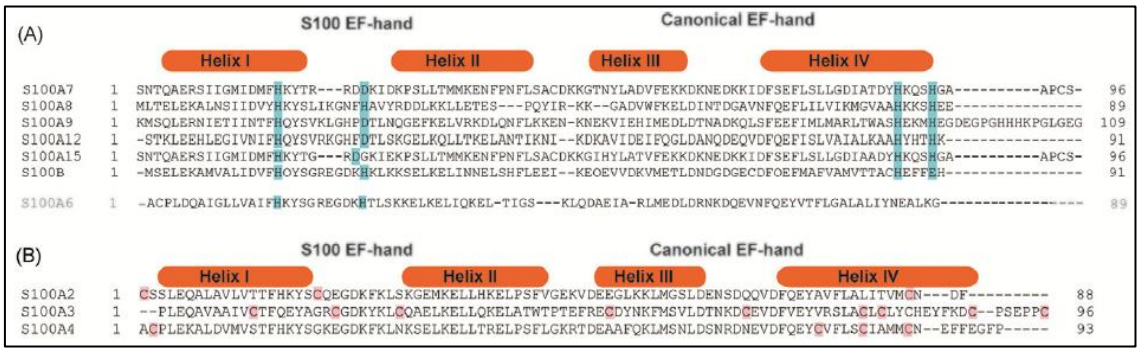

Figure 1.2.3 – Alignments of S100 proteins containing transition metal binding sites. Structure based sequence alignment of S100 proteins from the (A) His-rich and (B) Cys-rich categories. Conserved residues in His-rich sites are highlighted with blue background, and those in Cys-rich sites in red background. Adapted from [82].

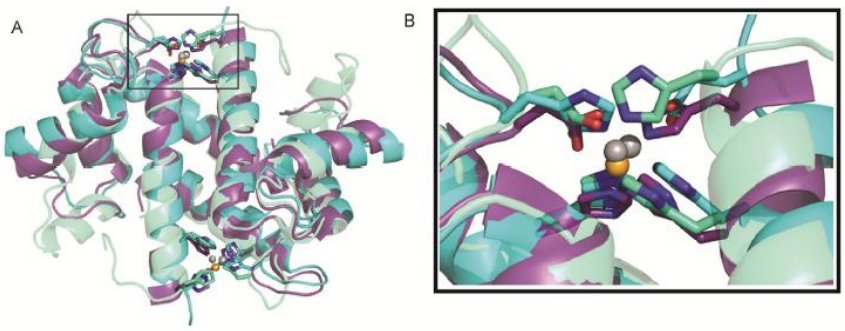

Figure 1.2.4 – Structural similarity of tetrahedral zinc and copper binding sites in S100 proteins. (A) Overlay of the structures of $(Ca^{2+})_4$, $(Zn^{2+})_2$-S100A7 (light green), $(Ca^{2+})_4$, $(Zn^{2+})_2$-S100B (blue) and $(Ca^{2+})_4$, $(Cu^{2+})_2$-S100A12 (purple) showing that the transitions metal ions are chelated in similar manner by side chains in the same position in the sequence. (B) Zoom in on the tetrahedral Zn^{2+} and Cu^{2+} sites showing the similar spatial disposition of the 3 His and 1 Asp chelating side chains. The Zn^{2+} and Cu^{2+} ions are colored gray and orange, respectively. Adapted from [82].

Regarding the Cys-rich Zn^{2+} binding S100 proteins (S100A2, S100A3, S100A4), these proteins are much less studied than the His-rich group [102], due to the absence of a conserved motif evident from alignment of these proteins

The possibility of different metals binding to an S100 protein, suggests scenarios where a crosstalk between metals that bind to S100 proteins is expected. In this context, it has been reported for the S100B that Zn^{2+} binding leads to an increase of the Ca^{2+} affinity by a factor of 10 and for the S10012 by ~1500 fold [102]. On the other hand, it lowers the Ca^{2+} affinity of S100A2 [85] and have no effect on S100A5 [103].

Due to Cu^{2+} and Zn^{2+} similar chemical properties, it was expected that Cu^{2+} would bind to most zinc binding sites in proteins. Moreover, ion competition experiments demonstrated that the Cu^{2+} ions could be displaced by Zn^{2+}, but not Ca^{2+}. Thus, as expected, the S100 proteins bind Cu^{2+} in a similar way they bind Zn^{2+}. There is still few information about the effects of Cu^{2+} binding on S100 proteins, but it seems that the overall conformational change induced by the binding of Cu^{2+} is very small compared with Ca^{2+} or Zn^{2+} binding [82].

1.2.3. S100A9

The work developed in this thesis is about the S100A9 homodimeric form and how it reacts to binding of metals and aggregation conditions.

S100A9, also known as Mrp14, is a Ca^{2+}- and Zn^{2+}-binding protein with a molecular weight of 13.242 kDa, composed by 114 amino acids and has the longest C-terminal region in its sequence among the S100 family members (Figure 1.2.6). S100A9 is one of the most potent pro-inflammatory protein in the S100 family, being overexpressed in several inflammation scenarios, including inflammation associated with Alzheimer's disease [104].

The S100A9 is one of the major constituents of neutrophils which plays an important role in the regulation of inflammatory and immune response [105]. This protein exists preferentially as a heterodimer or heterotetramer with S100A8 known as calprotectin [106, 107]. However, it can also exist as homodimer [108] and higher oligomeric species, including, fibrillary structures due to its intrinsic amyloidogenicity [91]. Dimerization is achieved by anti-parallel interactions between helices H1 and H4 of each monomer (Figure 1.2.6) [108]. Each of these forms assumes specific functions and their formation is dependent on binding of divalent cations, such as calcium and zinc [108].

Current research on this protein is focused on its association with numerous human disorders, including acute and chronic inflammatory conditions, autoimmune diseases, cancer, atherosclerosis, cardiomyopathies and neurodegenerative diseases [104, 106-108], given its crucial role in normal physiological processes within cells.

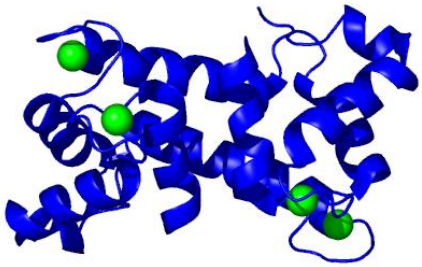

Figure 1.2.5 – S100A9 homodimer crystal structure (CHAPS removed). The Ca^{2+} ions are colored green. Images generated in pymol using PDB entry 1IRJ.

Primary Structure, Ca^{2+}- and Zn^{2+}-Binding Sites

Like other S100 proteins, S100A9 contain two EF-hand Ca^{2+}-binding sites: a C-terminal canonical EF-hand (site II) and a N-terminal pseudo EF-hand (site I) with a 12 and 14 amino acid residue Ca^{2+}-binding loop positioned between two supporting α-helices, respectively (Figure 1.2.6) [108]. The alignment of these motifs with other members of the S100 family has demonstrated that in both sites S100A9 contains the conserved sequence determinants required for Ca^{2+}-binding [108].

The Ca^{2+}-binding site II include residues Asp67-Glu78 and interacts with Ca^{2+} through seven oxygen ligands, forming a pentagonal bipyramidal coordination: the side-chain O atoms of Asp67, Asn69, Asp71 and Glu78, the main-chain carbonyl O atom and a water molecule. The Ca^{2+}-binding site I include residues Ser23–Glu37 and interacts with Ca^{2+} through seven O atoms from the main-chain carbonyl groups of Ser23, Leu26, His28 and Thr31, the carboxyl group of Glu36 and a water molecule (as indicted in Figure 1.2.6) [108]]. The water molecule as a seventh ligand also forms a hydrogen bond with the side-chain of Thr31.

Although it is know that S100A9 is important for Ca2.-dependent functions during inflammatory conditions, the function behind the Ca^{2+}-S100A9 interaction is yet to be unveiled [108]. However, it has been shown that Ca^{2+} is capable of inducing S100A8/A9-tetramerization [109].

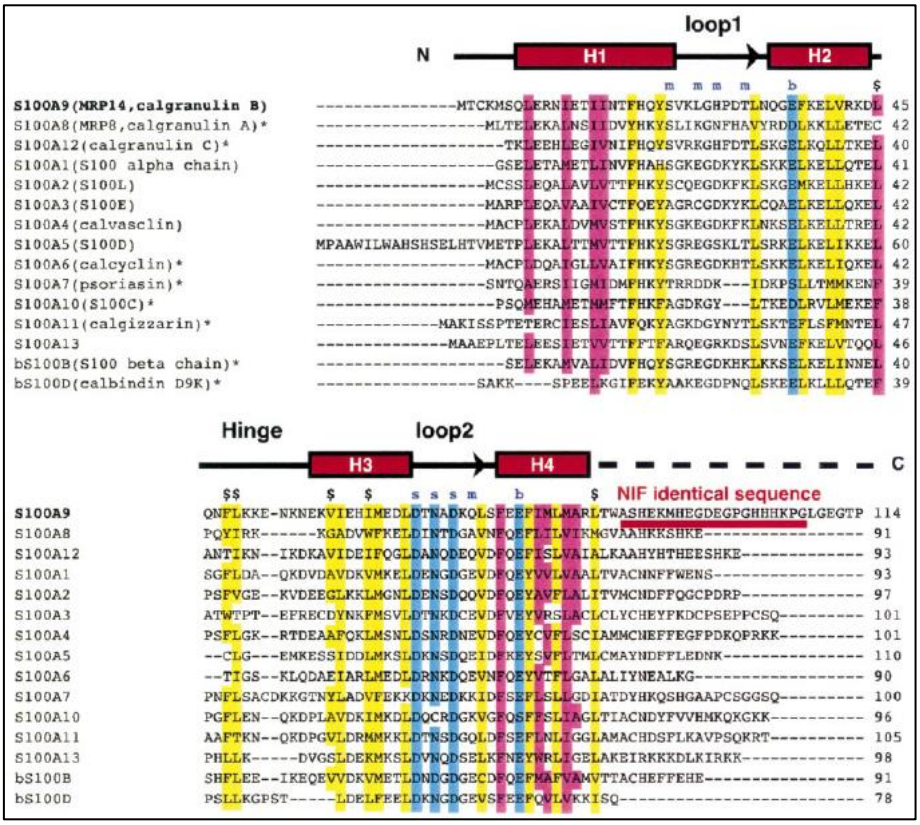

Figure 1.2.6 – Amino acid sequence alignment of the human S100 family of proteins. Proteins whose three-dimensional structures have already been analysed are marked by an asterisk. Secondary structure elements of S100A9 are given. Residues that coordinate calcium ions are marked as follows: m, main-chain carbonyl group; s, mono-dentate side-chain of Asp or Asn; b, bi-dentate side-chain of Glu. The residues highlighted in blue are well-conserved residues the side-chains of which coordinate calcium ions. The residues highlighted in yellow represent highly conserved hydrophobic residues forming an intra-monomer hydrophobic cluster. Residues that interact with target molecules are marked with $. The residues highlighted in pink are other conserved hydrophobic residues that form an inter-monomer hydrophobic cluster. All sequences were obtained from the SWISS-PROT protein sequence database [110]. Adapted from [108].

Besides Ca^{2+}, S100A9 also bind Zn^{2+} ions. S100A9 is classified in the his-rich category of the Zn^{2+} binding S100 proteins and contain HEXXH motives in its sequences that are putative Zn^{2+}-binding sites [111].

The role of zinc in S100A9 is still unclear, however it has been reported that S100A9 chelates zinc as a biological function [112]. Moreover, different biophysical methods have shown that Zn^{2+}-induces S100A8/A9-tetramerization by binding to both Ca^{2+}-specific EF-hands and Zn^{2+}-specific binding sites [113, 114]. The researchers who carried out this study reported that twelve Zn^{2+} were bound to the tetramer (eight Zn^{2+} bound to the EF-hands and four Zn^{2+} to the Zn^{2+}-specific binding sites) [113, 114], revealing the existence two different putative Zn^{2+}-binding sites on the S100A8/A9 subunit interface.

Interestingly, several other S100 family members are also regulated by Zn^{2+} and Ca^{2+} [115], as mention earlier, and for some of them the Zn^{2+}-binding sites have been well characterized (S100B, S100A2, S100A7 and S100A12) by different techniques [116, 117]. For these proteins it was observed the binding of two Zn^{2+}-ions per homodimer and that both subunits provide residues to form the Zn^{2+}-binding sites. Since the Zn^{2+}-binding residues in S100A9 and S100A7 are fully conserved, it is likely that the S100A9 homodimer coordinates Zn^{2+} in a similar way as S100A7 [86, 118].

1.2.4. S100A9 in Alzheimer's disease

As aforementioned, S100A9 is involved in several human disorders, including Alzheimer's disease (AD). AD is a neurodegenerative disorder characterized by the accumulation of amyloid-β protein (Aβ) in extracellular plaques and the deposition of hyperphosphorylated tau protein in intracellular neurofibrillary tangles [119-121], which are directly associated with prominent neuroinflammation [122]. In turn, this condition is correlated with a severe deterioration of cognitive function [123], however the molecular mechanisms underlying this observation are yet to be unveiled [124, 125]. Furthermore, aberrant metal homeostasis seems to be related with AD pathogenesis [126].

S100A9 plays an important role in regulating vascular inflammation, by recruiting leukocytes to damaged vessels, such as those injured by deposition of Aβ amyloid fibrils [127]. Moreover, an overexpression of S100A9 has been reported in microglia in the temporal cortex of both familial and sporadic AD cases [128], suggesting that S100A9 could be a neuroinflammatory marker of AD.

The accumulation of Aβ amyloid fibrils on cerebral vessels and in brain parenchyma leads, consequently, to local inflammation [129], which in turn results in activation and recruitment of microglia to the plaque deposition site [130], causing microgliosis. From this point, microglia acts in two ways: beneficial promotion of phagocytosis of Aβ and harmful production of neurotoxins and pro-inflammatory molecules [131-133], such as S100A9. The high levels of S100A9 on Aβ amyloid fibril deposits promotes further inflammation and enhances Aβ amyloid fibrils formation. Moreover, S100A9 drives microglia into a pro-inflammatory state thereby compromising microglial phagocytosis [131, 134].

Among this events, BACE1 activity is also elevated, resulting in increased Aβ production [135], which in turn further accelerate S100A9 expression, creating a vicious cycle that promotes and expands the deposition of Aβ amyloid fibrils including amyloid-associated proteins on cerebral vessels and in brain parenchyma (Figure 1.2.7).

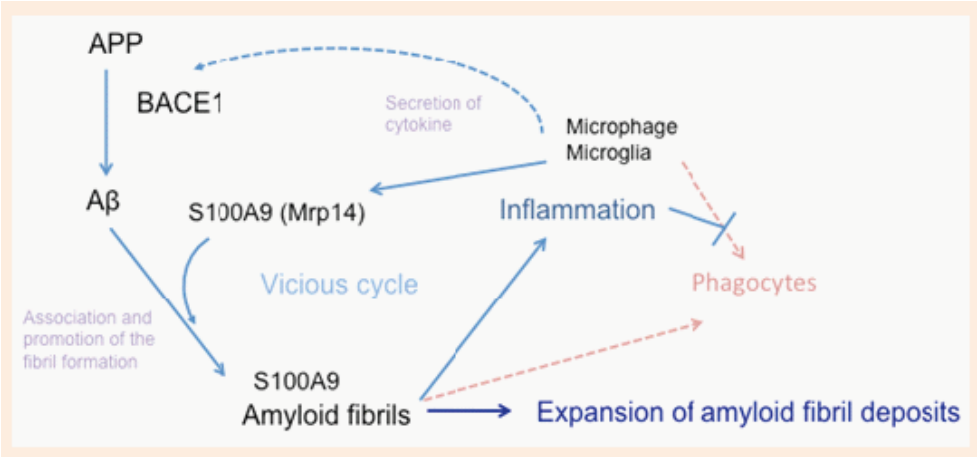

Figure 1.2.7 – A comprehensive model of amyloid fibril formation enhancement. Local inflamation by Aβ amyloid deposition induces S100A9 production by activated phagocytes and up-regulation of the inflamatory condition. Thereafter, S100A9 induces increased formation of Aβ amyloid fibril and futher inflamation. Moreover S100A9 drives microglia into proinflamtory state thereby compromising microglial phagocytosis. Adapted from [136].

Due to its inherent amyloidogenicity, the significantly increased levels of extracellular S100A9 leads to its amyloid aggregation [137-139] and also co-aggregation with Aβ [140], enhancing each other aggregation, suggesting a "rescue" clearance process to remove neurotoxic amyloid species from circulation. However, the consequences of this clearance process can lead to exacerbated growth of the amyloid plaques in AD brain, much more stable and protease resistant [91]. Furthermore, the plaques themselves can lead to more microglia activation, thus completing the vicious circle of amyloid-neuroinflammatory cascade.

Interestingly, the knockdown or knockout of the S100A9 gene in AD mice model (Tg2576) significantly reduced the neuropathology and the amount of Aβ, C-terminal fragments of amyloid precursor protein (APP-CT) and phosphorylated tau [141].

Therapeutic strategies for AD treatment focus on inhibiting Aβ production and/or enhancing Aβ clearance [136]. Therefore, due to its amyloidogenicity, neurotoxicity and signaling functions, S100A9 may be a promising therapeutic target. However, the specific role of S100A9 in AD as well as in aging is still far from clear.

1.3. Methods for structural analysis and protein folding monitoring

1.3.1. Fluorescence spectroscopy

Fluorescence spectroscopy is an important investigation tool in different areas of analytical science, due to its high sensitivity and selectivity. Its applications include the study of protein folding, structural dynamics and protein interactions by monitoring the tertiary structure of proteins [142]. For many proteins this application is possible due to their intrinsic fluorescence granted by the presence of aromatic amino acid residues, such as the tryptophan (Trp), tyrosine (Tyr) and phenylalanine (Phe). These residues and other fluorescent molecules are called fluorophores. Besides intrinsic fluorophores there are some extrinsic probes that also give information about the protein folding, misfolding and ultimately amyloid formation. The probes used in this work were: Thioflavin-T (ThT); 8-anilino-1-naphthalenesulfonic acid (ANS); and two luminescent conjugated oligothiophenes (LCOs), p-FTAA and h-FTAA.

ThT is a benzothiazole dye that exhibits enhanced fluorescence upon binding to amyloid fibrils. Originally, it was thought that ThT only interacted with the amyloid cross-β structure [143], however, it has been shown that ThT fluorescence can bind to non-β-sheet cavities (observed for acetylcholinesterase and γ-cyclodextrin) [144]. The binding leads to an increase in fluorescence intensity and induces a shift in the maximum wavelength from 483 nm to 478 nm [145].

ANS is known to interact with hydrophobic sites, such as the ones buried within the protein. For this reason this probe has been widely used in protein folding and binding studies, where sometimes hydrophobic regions exposure occurs. Once more, this interaction leads to an increase in fluorescence intensity and induces a shift in the maximum emission wavelength, from 530 nm to 475 nm [142].

LCO's are anionic oligothiophene based ligands capable of detecting non-thioflavinophilic aggregated species preceding amyloid fibril formation. They presumably intercalate with the amyloid fibrils by binding in grooves along the long axis of the amyloid fibril [146]. The ones used in this work where the p-FTAA and h-FTAA, each with distinct spectral signature. The binding of this probes leads to the increase of their fluorescence intensity [146].

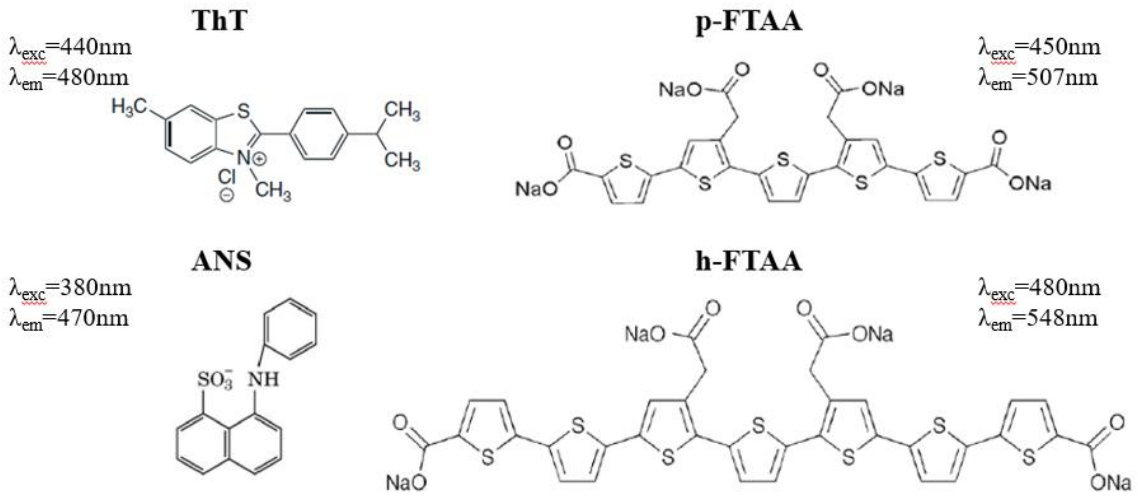

Figure 1.3.1 – ThT, ANS, p-FTAA and h-FTAA chemical structures and respective excitation emission wavelengths.

1.3.2. Conformation studies by Imunodetection

The formation of amyloid deposits is a characteristic feature of many degenerative disease and its staining in human and mice AD brains has been a challenge. However, it has been overcome by the development of conformation-dependent antibodies that specifically recognize generic epitopes of a polypeptide chain with given conformation, regardless of its sequence. This antibodies include the OC and A11. The OC antibody recognizes amyloid fibrils, while the A11 specifically recognizes a generic epitope common to prefibrillar oligomers [147, 148].

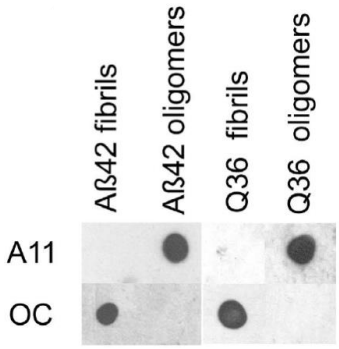

Figure 1.3.2 - Dotblot resulted from detection of fibrils and oligomers, from different proteins, by the conformation-dependent antibodies A11 and OC [148].

1.3.3. Atomic Force Microscopy

Atomic Force Microscopy (AFM) is the most versatile and high-resolution scanning method for studying samples at nanoscale. An AFM uses a cantilever with a sharp tip to scan samples adsorbed on atomically flat smooth surfaces, typically mica. As it goes along the surface the cantilever deflects vertically and laterally producing a signal which is translated to generate a corresponding topography image. This technique has been used to investigate the self-assembly dynamics of several amyloidogenic proteins and other types of aggregates [149].

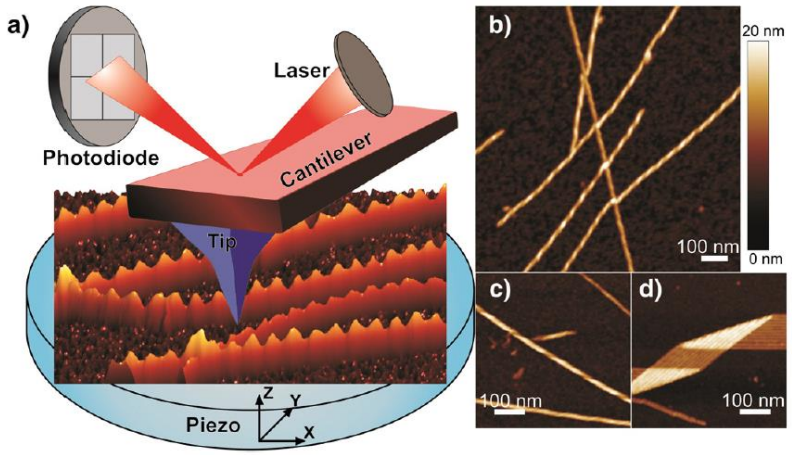

Figure 1.3.3 - The operating principle of AFM and AFM images of amyloid fibrils. a) Schematic representation of AFM measurement. AFM image of b) twisted ribbons, c) helical ribbon d) multi-stranded helical fibril. Adapted from [149].

1.4. Objectives

Metal ions have prominent as regulators of structure and function of S100 proteins, whose functional and amyloid-type oligomerization has been implicated in pathophysiological processes related to neurodegeneration. This work aimed at investigating the metal-ion dependent oligomerization of the pro-inflammatory S100A9 protein, in an attempt to gain insights into understanding how binding of zinc and calcium influence its self-assembly. Specific objectives included:

- Obtaining highly pure preparations of human homodimeric S100A9 protein through recombinant expression, chromatographic purification, and preparation and biochemical characterization of apo-forms;
- Comprehensive analysis of the S100A9 self-assembly reaction in the presence of Ca^{2+} and Zn^{2+} using fluorescence based kinetic assays and extrinsic dyes;
- Conformational characterization of S100A9 oligomers and aggregates combining biophysical, biochemical and immunological approaches.

The work reported in this thesis was carried out in the research laboratories of the 'FCUL Protein Folding and misfolding laboratory' (http://folding.fc.ul.pt/) which is affiliated to BioISI – Biosystems & Integrative Sciences Institute and is located at the FCUL Chemistry and Biochemistry Department (C8 building FCUL campus). The AFM measurements and analysis was performed by collaborators at the BioISI Magnetic Nanosystems Group / Department of Physics, also at FCUL (see acknowledgments).

II. Materials and Methods

2.1. Expression and purification

2.1.1. S100A9 homodimer expression and purification

The following expression and purification steps were adapted from [114]. The recombinant human S100A9 was expressed in *E.Coli* BL21 (DE3) cells transformed with a plasmid containing the S100A9 gene. The first step of the expression was the preparation of a pre-inoculum, where a previously prepared glycerol cell culture stock was added to a DYT medium, supplemented with 100 mg/mL ampicillin and 20% (m/v) glucose, and incubated overnight at 37 °C with 150 rpm agitation. From this pre-inoculum, 10 mL were transferred to a 0.5 L DYT medium, supplemented with 100 mg/mL ampicillin and 20% glucose and incubated at 37 °C with 150 rpm agitation until OD_{600} = 1 was achieved. At this point expression was induced by adding 0.5 mM of IPTG. After 4h of incubation, the cells were harvested by centrifugation (JA-14 rotor) with 8000 rpm for 10 min at 4°C and then frozen.

The purification step begins with the resuspension of the cells in 20 mM Tris-HCl pH 8, with DNase (for DNA degradation) and 0.5 mM of PMSF (to inhibit proteases). After solubilization, cells were broken by sonication (50% amplitude and 0.5 on/off cycles, during 10 min) and then centrifuged (JA-25.5 rotor) at 16000 rpm for 20 min. The supernatant was discarded and the pellet resuspended in 20 mM Tis-HCl pH 8, 10 mM EDTA, 0.5% (v/v) Triton X-100 followed by sonication and centrifugation in the same conditions as above, obtaining the inclusion bodies. The pellet obtained from this centrifugation was resuspended in 6 M guanidine-HCl, with the help of a membrane homogenizer, in order to extract the proteins from the inclusion bodies. After 1h, the extract was diluted with 20 mM Tris-HCl pH 8, 1 mM EDTA, 1 mM EGTA and 0.5 mM DTT in order to decrease guanidine-HCl concentration to 1 M. This extract was then centrifuged (16000 rpm, 20 min), the supernatant collected, filtered and loaded into a desalting chromatography column (HiTrap desalting) to separate the proteins from guanidine. Afterwards, the fractions obtained that corresponded to proteins were loaded into a size-exclusion chromatography column (Superdex 75 16/600) against 20 mM Tris-HCl, 1 mM EDTA, 1 mM EGTA, 150 mM NaCl pH=8 and 0.5 mM DTT. Using the calibration curve from this column it was possible to discriminate which fractions contained S100A9 homodimer. At last, those fractions were then passed through an ionic-exchange chromatography column with an ionic gradient from 0 to 1 M NaCl. The two elution buffers for this final step were A: 20 mM Tris-HCl pH=8, 1 mM EDTA, 1 mM EGTA, 0.5 mM DTT and B: Tris-HCl pH=8, 1 mM EDTA, 1 mM EGTA, 0.5 mM DTT, 1 M NaCl.

Since the beginning of the purification, extracts were always kept on ice and the chromatography steps were made in a cold chamber at 4ºC.

2.1.2. S100A9 demetalation

In order to remove possible metal ions bound to the protein, S100A9 was incubated 2 hours at 37°C, in presence of dithiothreitol (DTT) 300-fold protein concentration (redox reagent) to avoid possible disulfide bond formation and 0.5 mM of ethylenediaminetetraacetic acid (EDTA) to chelate metal ions. After incubation, protein sample was loaded into a size-exclusion chromatography column (Superdex 75 10/300 GL, GE Healthcare, V_{column}=24 ml) with 50 mM Tris-HCl pH 7.4, prepared with metal-free water (chellex water), to separate existing multimers formed during incubation, DTT and EDTA, obtaining pure S100A9 demetaled (apo form).
Protein was then stored at -4ºC in concentrations ranging from 80 to 120 µM.

2.1.3. Determination of S100A9's concentration

Since S100A9 has aromatic residues it can absorb UV light at 280 nm. So, knowing the extinction coefficient (ε) for S100A9 monomer protein (ε^{280nm}= 6,990 $M^{-1}.cm^{-1}$), we could measure the absorbance in a UV/Vis spectrometer and calculate the protein's concentration protein using Beer-Lambert's law (A = εlc, where l is the path length of the spectrometer). Considering that we worked with S100A9 homodimer, it was required to multiply ε by 2 to calculate the homodimer concentration.

Other method used to determine protein's concentration was the Bradford method, which is a colorimetric assay based on the interaction between Coomassie brilliant blue and the arginine and aromatic residues in your protein, which leads to shift in its maximum absorption from 470 nm to 595 nm. By creating a standard curve with the absorbance of a series of known concentrations of BSA, we can used it to calculate the concentration of our protein sample based on its absorbance. Samples were prepared by mixing 600 µL Bradford reagent (0.1 mM Coomassie Blue, 4.75% ethanol, 8.5% (m/v) phosphoric acid) with 20 µL of protein sample.

2.1.4. Electrophoresis

Since S100A9 has a molecular weight of ~13 kDa it was required to make gels with higher resolution/separation for smaller proteins. To do so we prepared a Tris-Tricine SDS-PAGE gel. First, the resolving gel was prepared with 8% of acrylamide/bis-acrylamide (29:1 solution), 1M Tris 0.1% SDS pH 8.45, 0.05% of amonia persulphate (APS), 8 mM TEMED and finished my adding H_20. After polymerization of the resolving gel, the stacking gel was added (prepared with 3.2% acrylamide/bis-acrylamide (29:1), 0.67 M Tris pH 8.45, 0.067% SDS, 0.03% of APS, 13 mM TEMED and finished by adding H_20).

Samples were prepared by my mixing them with loading buffer (3% SDS, 5% 2-mercaptoethanol) in 1:1 ratio and incubated ~10min at 100 ºC to denature proteins. For the purpose of this method two running buffers were used: cathode buffer (0.1M Tris, 0.1M Tricine, 0.1% SDS with pH 8.25) and anode buffer (0.2M Tris, pH 8.9). The voltage used was 150V. After running the gels, these were stained with BlueSafe solution (Nzytech) for ~2 hours (no distaining required). When accurate concentration was necessary, samples were applied with 10µM.

2.2. Morphology, structural and kinetic studies

2.2.1. Aggregation Assays

Aggregation assays were performed by fluorescence spectroscopy through binding of different fluorescent probes: ThT (sigma); ANS; and the LCOs, p-FTAA and h-FTAA. The used probes concentration were 40 µM ThT, 100 µM ANS and 0.2 µM LCOs. Samples were prepared in 50 mM Tris-HCl pH 7.4 (in chellex water), in the presence of 5 mM TCEP and one of the probes. Protein concentration range went from 5 to 40 µM, but 20 µM was the concentration mainly used. These assays were also done in presence of metal ions, such as zinc (Zn^{2+}) and calcium (Ca^{2+}), whose concentrations ranged from 20 to 200 µM. The 96-well plates (black, clear bottom, Corning) were analyzed in the FluoStar Optima (BMG Labtech) and the excitation/emission filters used were 440/480 nm for ThT, 370/480 nm for ANS, 440/480 nm for p-FTAA. For the h-FTAA, there no filters available, so we used the Gemini EM Microplate Reader because it has a monochromator, which was set to 360/408 nm (excitation/emission). The kinetics were done with incubation temperature of 37 °C and 86 rpm agitation cycles of 20

seconds before each acquisition. In order to optimize each probe's signal to detect S100A9 assemblies, this probes were first tested in a fluorimeter and their spectra were acquired.

2.2.2. Turbidimetry

The aggregation of S100A9 in the presence of different zinc concentrations was determined by measuring the apparent absorbance at 360 nm caused by increased turbidity. The aggregation was followed in the FluoStar Optima (BMG Labtech), using 96-well transparent plates. Samples were prepared in 50 mM Tris-HCl pH 7.4 (in chellex water), in the presence of 5 mM TCEP.

In each experiment, the total volume in per well was 200 µL and the aggregation was started by the addition of zinc. The apparent absorbance was measured as a function of time. The measurements were performed with incubation temperature of 37 °C and 86 rpm agitation cycles of 10 seconds every 3 min. The effects of EDTA addition to S100A9 metal-induced aggregates were also analyzed in this experiment.

2.2.3. Dot-blot Analysis

S100A9 conformational state was analyzed by its reactivity against conformation dependent antibodies was carried out in a dot-blot analysis as described in [148] using the anti-amyloid fibrils OC antibody (AB2286 Merck Millipore) and the A11 anti pre-fibrillar oligomers antibody (AB9234 Merck Millipore). Samples were analyzed after 25 hour incubation with Ca^{2+} and/or Zn^{2+}.

This experiment begins with the preparation of the PVDF membrane for blotting. Firstly, wet the membrane with 100% methanol for a few seconds, then with water and finally with transfer buffer (25 mM Tris, 192 mM Glicine, 10% methanol and 0.1% SDS), incubate 2-3 minutes. Next, samples were applied in each dot (5 or 10 µL) and left overnight. The second part begins with washing the blotted PVDF membrane twice with TBS-T buffer (50 mM Tris and 0.1% NaCl with 0.05% Tween) and then was blocked in TBS containing 5% non-fat dry milk for 30 min at room temperature with agitation. Afterwards, the blotted membrane was incubated with 1:1000 dilution of OC (10uL/10mL) antibody and 1:500 dilution of A11 (20uL/10 mL) for 2 h with agitation. Later, to remove the unbound antibodies the membrane was washed 4 times with TBS-T for 5 minutes each. Next, the membrane was incubate with HRP-coupled secondary antibody (5uL/10mL) in TBS-T milk for 1 hour with agitation and then, after this time, washed again 4 times in TBS-T for 5 minutes each. Finally ECL solution was used according to manufacturer (ECL Bio-Rad, mix equal volumes of solution A and solution B) for enhanced chemiluminescence and the result was visualized using the Chemidoc visualization system (Bio-Rad).

2.2.4. Atomic force microscopy (AFM) assay

Aggregated protein samples were deposited on the surface of freshly cleaved mica (Agar Scientific) for 10-30 min, washed 3 times with 100 µL of deionized filtered water, to remove unwanted contaminants, and dried with a nitrogen source and then subjected to AFM analysis. The samples were prepared from different time points of the aggregation kinetic obtained in distinct conditions. The volume applied on mica was 20 µL with a final concentration of 1 µM.
The AFM measurements and analysis was performed by collaborators at the BioISI Magnetic Nanosystems Group / Department of Physics, also at FCUL (see acknowledgments).

2.2.5. Analytical size exclusion chromatography (SEC)

Analytical SEC was performed at room temperature on a Superdex 75 Tricorn high performance column (GE Healthcare, V_{column} =24 ml) connected to an AKTA Purifier UPC-10 system and run at 1 ml/min. The column was calibrated with proteins of known molecular weight: ribonuclease A (13.7 kDa), cytochrome c (11.8 kDa), carbonic anhydrase (29 kDa), ovalbumin (43 kDa) and albumin (67 kDa). Calibration curve is the appendix section (Figure 2.2.1**Erro! A origem da referência não foi encontrada.**). Samples were incubated 25 h at 37 °C with 250 rpm agitation. Before injection (V_{inj}= 500 µL), samples were centrifuged 5-10min with 14000 rpm. The running buffer was 50 mM Tris-HCl pH 7 with 30 mM NaCl.

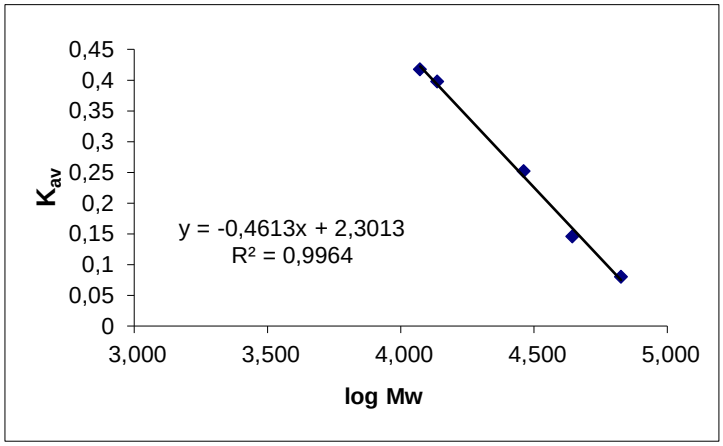

Figure 2.2.1 - Calibration curve used for S100A9 self-assembly analysis by SEC.

III. Results and Discussion

3.1. Purification of S100A9 homodimer

Protein purification relies on the knowledge about the protein's characteristics, such as size, isoelectric point (pI) and interactions. The expression and purification of S100A9 homodimer was adapted from [114] and optimized in previous work in our laboratory. In order to obtain pure S100A9 homodimer a series of processes to isolate the protein have to be done, as depicted in the diagram below (Figure 3.1.1).

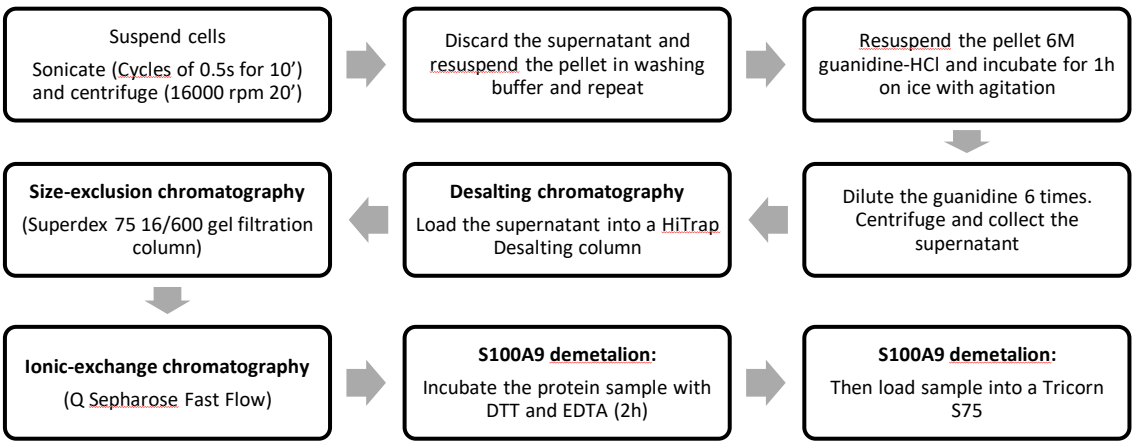

Figure 3.1.1 – Diagram of purification steps for S100A9 homodimer.

In the first part of the purification 15g of *E. coli* cells expressing recombinant human S100A9 underwent a sequence of steps in order isolate inclusion bodies and then extract the proteins within, including S100A9, by adding guanidine. This extract was then submitted to a desalting chromatography to separate proteins from the guanidine since the prolonged presence of this compound may permanently lead to protein misfolding. The result of this step can be observed below (Figure 3.1.2).

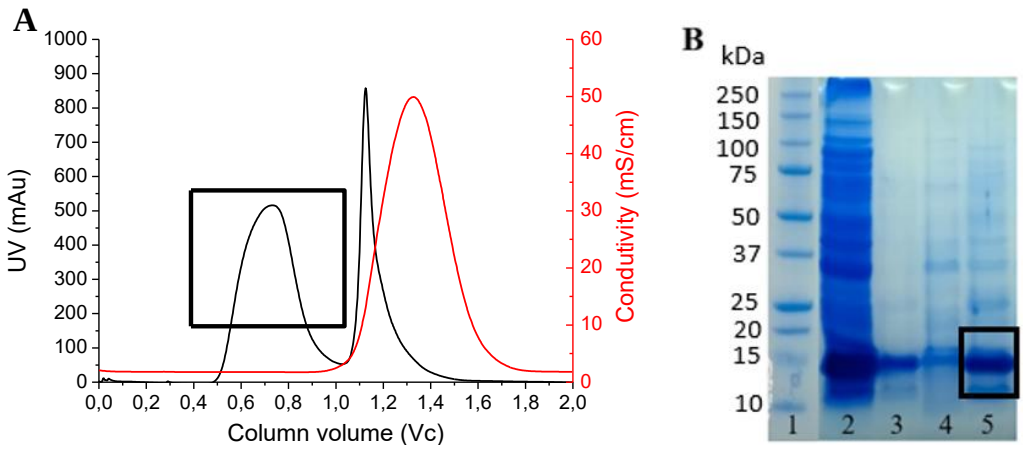

Figure 3.1.2 – Desalting chromatography purification step. (A) Chromatogram with Abs_{280nm} vs elution volume (Ve). (B) SDS-PAGE: 1-standarts; 2-protein extract injected; 3-fractions from 2nd peak; 4-fraction from between peaks; 5-fraction from 1st peak.

The conductivity of the solution (red curve) increases when guanidine passes through the sensor, providing an easy way to discriminate the presence of this compound. As depicted in Figure 3.1.2 B lanes 2, 3 and 4 from the SDS-PAGE gel shows that this step was successful and now proteins are free from guanidine (black square), although some were retained in the guanidine fractions.

Afterwards, the protein extract was loaded into a size-exclusion chromatography column. Knowing that S100A9 homodimer has a molecular weight of approximately 26 kDa and using the calibration curve of the column (Figure 3.1.3 B) it was possible to predict which fractions contained S100A9 homodimer (Figure 3.1.3).

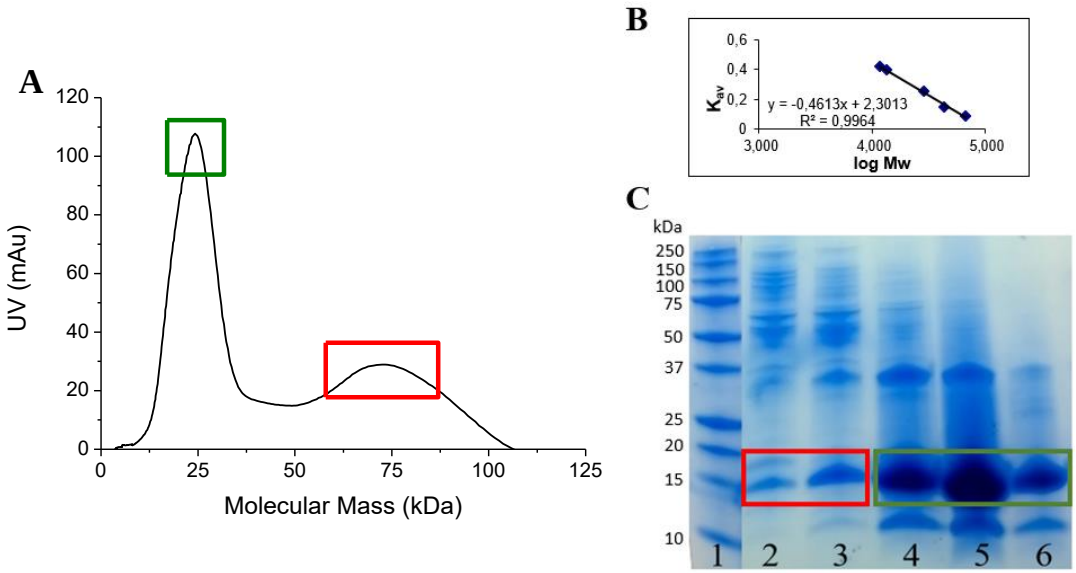

Figure 3.1.3 - Size-exclusion chromatography purification step. (A) Chromatogram with Abs_{280nm} vs elution volume (Ve). (B) Calibration curve for the size-exclusion chromatography column used in purification of S100A9. (C) SDS-PAGE with different fractions of this step: 1-standarts; 2,3-fractions from 2nd peak (red square); 5,6,7- fractions from 1st peak (green square).

In the chromatogram depicted above in Figure 3.1.3 are represented the different peaks that contain a variety of proteins separated by size. According to the calibration curve the elution of S100A9 homodimer occurs at a specific column volume, which strikingly corresponds to the highest peak in Figure 3.1.3 A (green square). This assumption was further confirmed by SDS-PAGE (Figure 3.1.3 B). The presence of S100A9 in the second peak was believed to be an S100A9 hexamer (red square), according to the calibration curve, formed during the purification initial steps.

Lastly, the fractions collected were then passed through an ionic-exchange chromatography column with an ionic gradient from 0 to 1M NaCl. The results from this step are represented below (Figure 3.1.4).

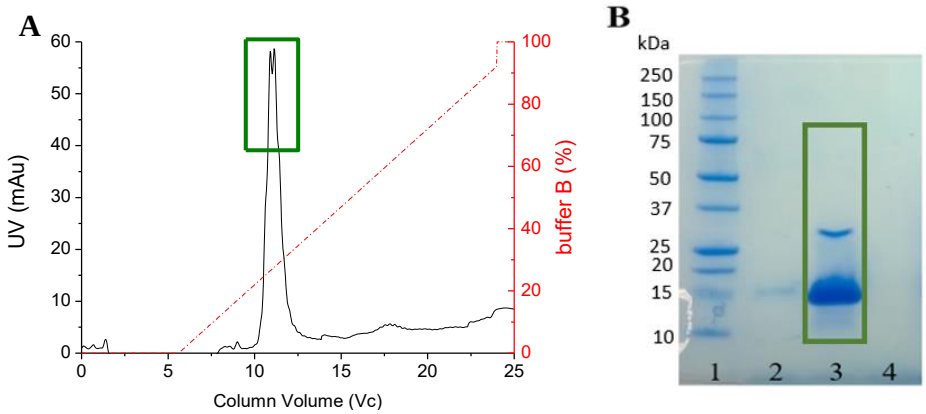

Figure 3.1.4 – Ionic-exchange chromatography purification step. (A) Chromatogram with Abs_{280nm} (black line) and buffer B % (red line) vs elution volume (Ve). (B) SDS-PAGE showing purified S100A9 homodimer.

The S100A9 homodimer was eluted at 28% of buffer B, i.e. 280mM of NaCl, and by analyzing the SDS-PAGE gel in Figure 3.1.4 B, it is evident that the eluted protein is highly pure.

Given that the main aim of this study was to evaluate the effect of metal ions (Ca^{2+} and Zn^{2+}) on S100A9, it was necessary to demetale the protein. Therefore, the sample was incubated with DTT and EDTA and then loaded into size-exclusion chromatography column in order to obtain purified metal-free S100A9 homodimer (apo form). The amount of protein purified was approximately 110 mg, giving a total yield of 7 mg protein/g cells.

3.2. Zinc and Calcium binding effects on S100A9 aggregation

S100A9 is a Ca^{2+}- and Zn^{2+}-binding protein highly abundant in the brain which has been reported to be overexpressed in many inflammatory conditions [89]. Moreover, it has been proposed that due to its inherent amyloidogenicity, high levels of extracellular S100A9 leads to its amyloid aggregation [137-139]. This protein can assume different forms: dimer, tetramer and larger oligomers, such as fibrillary structures [91]. The formation the different structures is thought to be dependent on metal-binding. For this reason, it is of great importance to study the interplay between Ca^{2+}- and Zn^{2+}-binding to S100A9 and how they affect oligomerization.

3.2.1. Analysis of the formation of zinc-dependent aggregates

In order to test the self-assembly of the S100A9 homodimer, aggregation assays were performed and analyzed kinetically by fluorescence spectroscopy through binding of ThT, a probe used specifically for detection of amyloid structures [143].

Firstly, we wanted to investigate if Zn^{2+} binding to S100A9 influences its self-assembly reaction. Hence, we tested the effect of Zn^{2+} in excess conditions (4Zn:S100A9), according to [108], and different S100A9 concentrations to uncover the critical concentration to aggregate (Figure 3.2.1).

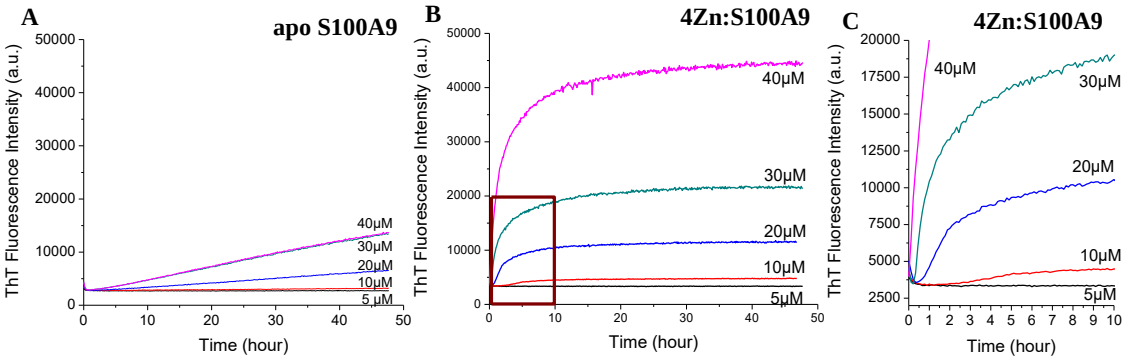

Figure 3.2.1 – Zn^{2+} enhances apo-S100A9 aggregation. (A) apo-S100A9 concentration gradient. (B) effect of 4Zn on the same S100A9 concentration gradient. (C) Zoom of red section marked in B

Interestingly, when comparing the free-zinc scenario (panel A) with the presence of $4Zn^{2+}$ (panel B) from Figure 3.2.1 we observed that Zn^{2+} is capable of inducing S100A9 self-assemble and formation of ThT-positive structures. However, this does not confirm that amyloid structures are formed. Indeed ThT is known to bind β-sheet-rich and non-β-sheet cavities [144]. In panel B can be observed that the classic sigmoidal curve did not occur but instead it seems to be almost exponential, with a barely existent lag phase, a characteristic of remarkable fast aggregation. This aggregation occurred only for S100A9 in concentrations above 10μM, being the critical concentration for S100A9 to aggregate in presence of Zn^{2+}. Furthermore, higher protein concentration correlated with a higher fluorescence intensity, higher rate (higher slope) and a decrease in the lag phase, from ~2 hours (10μM S100A9) to what seems instantaneous (40μM S100A9), suggesting a faster formation of aggregates (Figure 3.2.1 C). In conclusion, the binding of Zn^{2+} leads to the enhanced aggregation of S100A9, in a concentration-dependent manner.

We stipulated 20µM of S100A9 as the concentration for the majority of the following experiments, since at this concentration the short lag phase (t~30min) and the transition to the elongation phase could be observed with detail.

Afterwards, we assessed the effect of Zn^{2+}'s concentration on S100A9 by making a gradient of Zn^{2+} from 0 to 8-fold relative to the protein concentration (Figure 3.2.2).

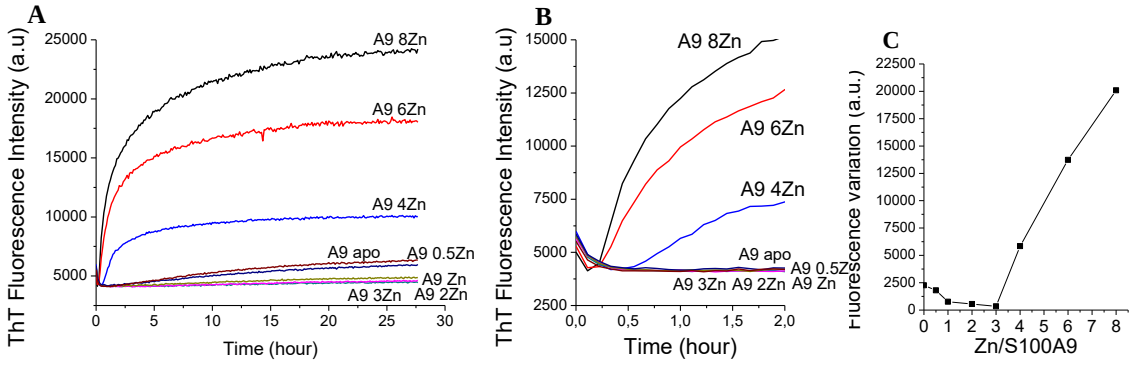

Figure 3.2.2 – Zn^{2+} gradient induces further aggregation. (A) S100A9 submitted to a Zn^{2+} gradient from 0 to 8-fold protein's concentration. (B) ThT fluorescence variation represented for each Zn/S100A9 ratio.

As depicted in Figure 3.2.2, the low ratios of Zn/S100A9, such as 0.5-3Zn/S100A9, were incapable of promoting S100A9 self-assembly. In fact, these ratios led to less ThT-binding than the apo form. For ratios above 4Zn/S100A9 an enhanced aggregation occurred, where the higher Zn content correlates with higher ThT fluorescence. Additionally, there was a simultaneous decrease of the lag phase and an increase of the slope, which are traits of a faster aggregation.

The Zn^{2+}-induced aggregates appeared, macroscopically, as a white precipitate (Figure 3.2.3 D), conferring a turbid appearance to the solution. As such, the solution's turbidity was measured at 360 nm in order to make correlations with the ThT kinetics. Both S100A9 and zinc's concentration gradients were used to better understand this Zn^{2+}-induced aggregation behavior. Zinc-free samples were prepared directly on the plate, and only after 30 minutes of measurements the Zn^{2+} was injected into each well with the desired concentration. Moreover, to see if the already formed Zn^{2+}-induced aggregates were reversible, we tested the effect of EDTA, a powerful chelating agent that is able to bind Zn^{2+} (added at t=12h).

On Figure 3.2.3 A, 20µM of S100A9 was titrated with Zn^{2+} ranging from 0 to 10-fold of S100A9's concentration. For ratios above 4Zn/S100A9 an instantaneous increase of turbidity was observed upon the addition of the metal. However, this phenomenon was only observed for concentrations of S100A9 above 10µM (Figure 3.2.3 B). Furthermore, the addition of EDTA at 12 hours successfully chelated Zn^{2+} and reverted the solution turbidity to its initial state. Figure 3.2.3 D shows, in a macroscopic point of view, the effect of EDTA displayed in the turbity kinetics, where is visible the regain of solution's transparency.

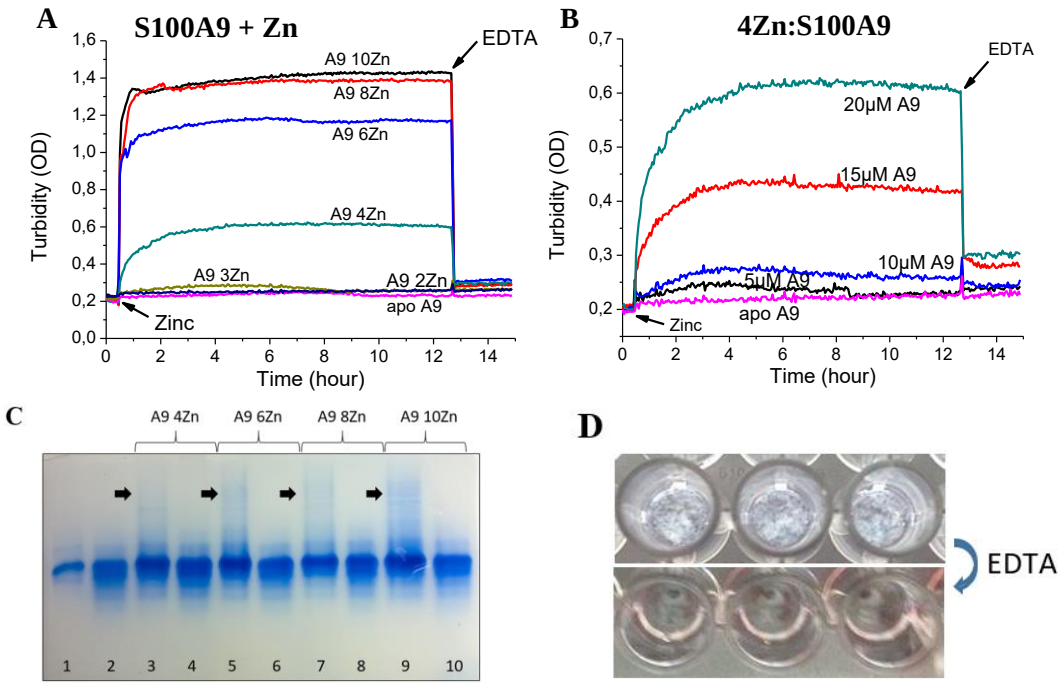

Figure 3.2.3 – Zn^{2+}-dependent aggregates formation and its reversion by EDTA. (A) Zn^{2+} gradient over S100A9. (B) Effect of 4Zn/S100A9 for different protein concentrations. (C) Native-PAGE of the S100A9 incubated samples with different Zn^{2+} concentrations. Each pair of wells has the samples before (wells 3, 5, 7 and 9) and after (4, 6, 8 and 10) addition of EDTA. Black arrows highlights smear. Apo-S100A9 was also loaded without (well 1) and with incubation (well 2) conditions. (D) Plate wells display solution's macroscopic appearance and the effect of EDTA.

Next, the aggregates formed in the experiment depicted in Figure 3.2.3 A were loaded into a Native-PAGE (Figure 3.2.3 C), before (black arrow) and after addition of EDTA to investigate the possibility that EDTA not only recovers solution transparency but also induces disruption of Zn^{2+}-induced aggregates. When comparing the well pairs, it's possible to observe that Zn^{2+} led to formation of a smear effect on the gel and that no other bands are visible. One could speculate that this smear results from S100A9 conformers induced by Zn^{2+} binding. In conclusion, adding to the previous results from ThT aggregation assays, zinc is capable of inducing S100A9 homodimer aggregation in a way that leads to the formation of insoluble ThT-reactive aggregates visible to a point where turbidity monitoring is possible. Formation of these aggregates is dependent on the 4Zn:S100A9 ratio and occurs strikingly fast. Furthermore, EDTA was capable of reversing the effect of Zn^{2+} in S100A9 aggregation. Additionally, ThT-binding displayed same EDTA behavior (Figure 3.2.4).

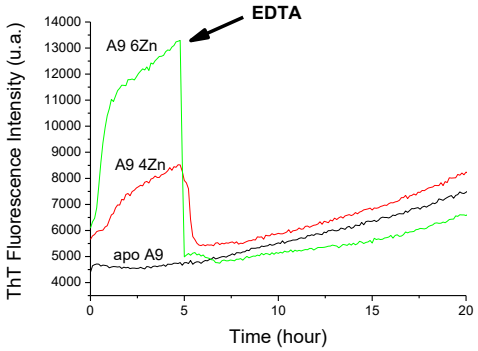

Figure 3.2.4 – ThT-kinetics show EDTA effect (added at 5 hours of incubation).

This type of aggregation could be driven by an electrostatic effect that alters protein solubility (salting out effect), however ThT-kinetics of S100A9 homodimer with excess of NaCl did not reproduce this aggregation (data not shown).

Afterwards, knowing that Zn^{2+} was able to induce S100A9 self-assembly, we wanted to investigate the morphology of the formed structures. For this purpose the S100A9 samples from the aggregation assays end points were analyzed by atomic force microscopy (AFM).

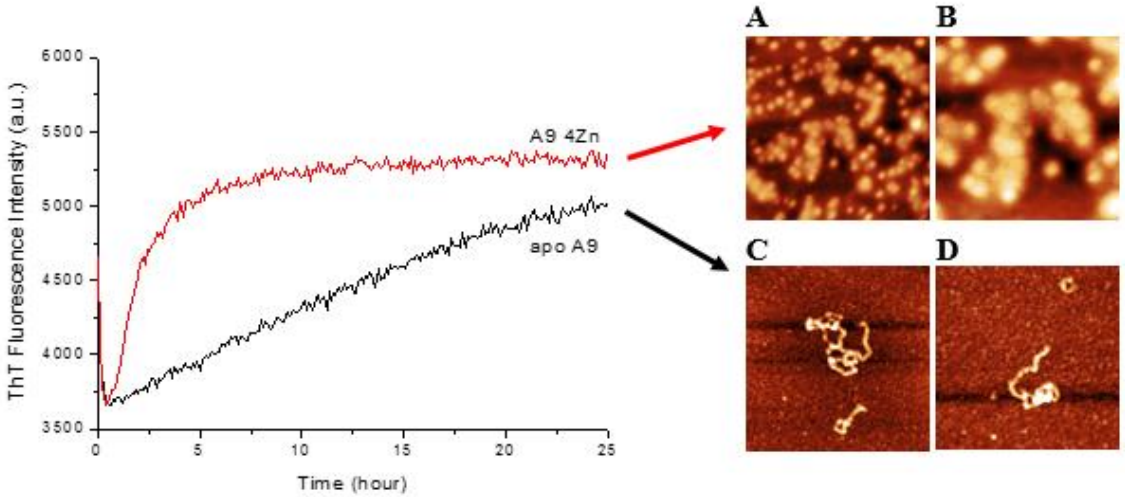

Figure 3.2.5 - Correlation between ThT kinetics and AFM imaging of apo S100A9 and 4Zn/S100A9 incubated 25h at 37ºC with 250rpm agitation. Panel (A) and (B) display the effect of Zn^{2+} on S100A9. Scan size of 2 and 1 µm, respectively. Panel (C) and (D) display apo S100A9 self-assembly. Scan size of 1 µm.

As depicted in Figure 3.2.5 A and B, imaging of incubated S100A9 in the presence of Zn^{2+} at a ratio of 4:1 showed that this condition induced the formation of amorphous aggregates with a flat sphere shape. Interestingly, statistics showed that this aggregates have a height of ~8 nm and a diameter of ~33.5 nm (data not shown), suggesting formation of structures with a size close to the tetramer [108]. The need of excess of Zn^{2+} to develop this structures might be explained by a study focused on S100A8/A9 where was reported that Zn^{2+} could bind not only to Zn^{2+}-specific sites but also to the Ca^{2+}-binding sites, inducing tetramerization [113, 114].

Regarding the metal-free S100A9, the images above (C and D) evidence the formation of different string-like structures with variable length.

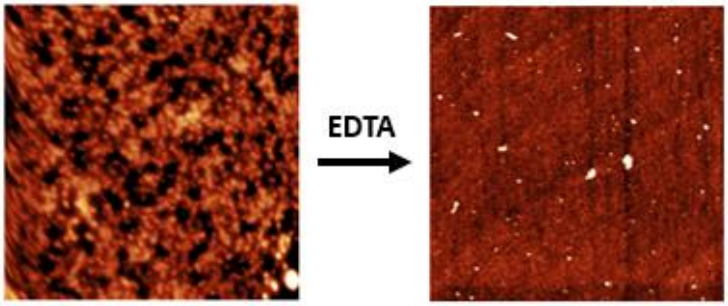

Figure 3.2.6 - AFM imaging of EDTA effect on Zn^{2+}-induced aggregates. Scan size of 5 µm.

We took advantage of AFM imaging to visualize EDTA effect on the Zn^{2+}-induced aggregates. In Figure 3.2.6 can be observed that EDTA led to the disruption of the Zn^{2+}-dependent aggregates, by chelating the Zn^{2+} bound to S100A9, in agreement with the observed loss of turbity and ThT emission decay.

As described earlier, a characteristic of amyloid formation is that this phenomenon can be triggered by seeding [47, 48] from existing aggregates. The kinetic changes induced by a seeding event include formation of larger aggregates and elimination of the lag phase. To test the effect of seeding, 25 hour incubation Zn^{2+}-induced aggregates were used to seed aggregation of S100A9 alone and in presence of Zn^{2+} at a ratio of 4:1.

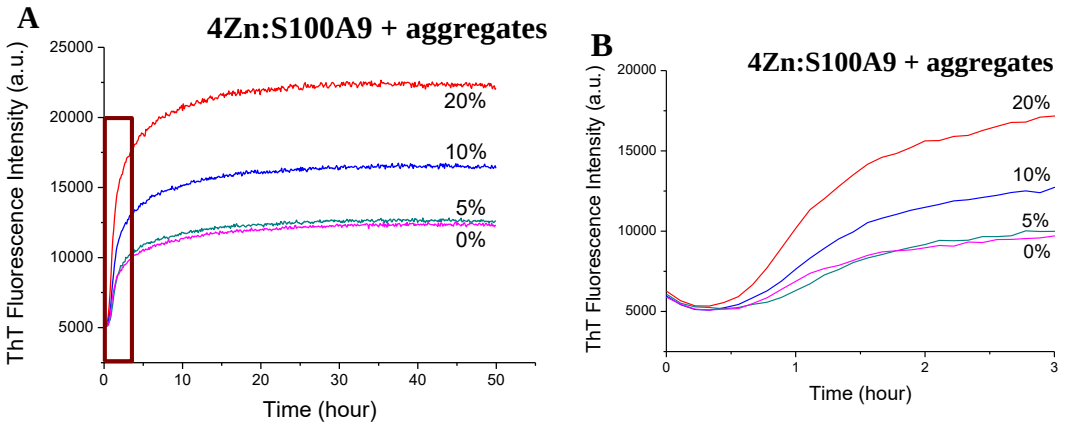

Figure 3.2.7 – Zn^{2+}-induced aggregates seed aggregation of 4Zn:S100A9. (A) 50 hour monitoring of seeding effect by adding 20%, 10% and 5% of aggregates. (B) Zoom of the first 3 hours (red section in A).

As it is depicted in Figure 3.2.7 A, seeding of 4Zn:S100A9 resulted in higher ThT fluorescence, as increasing amounts of aggregates were added. However, the lag phase seems unchanged (panel B). Moreover, in Figure 3.2.8 B, can be observed that the aggregates alone did not account for the gained ThT fluorescence observed, meaning that is not just adding fluorescence from individual events. On the other hand, seeding of apo S100A9 led to lower ThT reactivity (Figure 3.2.8 B), suggesting an interaction between the apo S100A9 and the Zn^{2+}-induced aggregates that resulted in a formation of ThT non-reactive species, possibly due to a stabilizing effect of the protein structure. Overall, the occurrence of seeding was not obvious and therefore we cannot conclude what happened to the aggregates, as they were not analyzed by AFM.

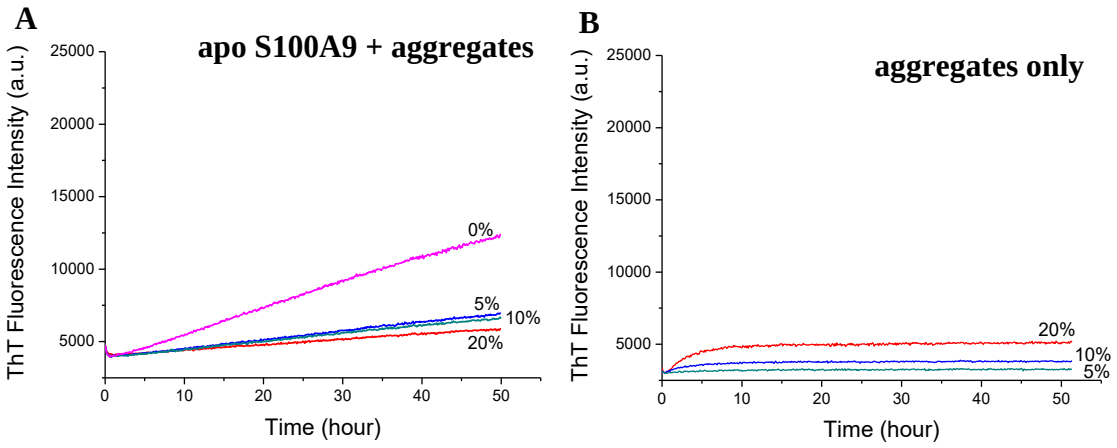

Figure 3.2.8 – No seeding effect on apo-S100A9. (A) Different amounts of Zn^{2+}-induced aggregates added to S100A9 homodimer. (B) Control - aggregates alone.

Aiming to shed light on the conformational changes induced by Zn^{2+} and to identify possible intermediate structures, different probes, such as ANS, p-FTAA and h-FTAA, were used to analyze S100A9 alone, in presence of 4:1 and 6:1 Zn/S100A9 ratio.

ThT is the probe mostly used to detect amyloid fibrils [143] but is has been shown to bind also to non-β-sheet cavities [144]. On the other hand, ANS is known to interact with hydrophobic sites, such as the ones exposed when protein starts to aggregate [142]. Lastly, p-FTAA and h-FTAA (LCOs), each with a distinct optical signatures, are capable of detecting non-thioflavinophilic aggregated species such as the ones preceding amyloid fibril formation, but how these probes interact is still to be explained [146].

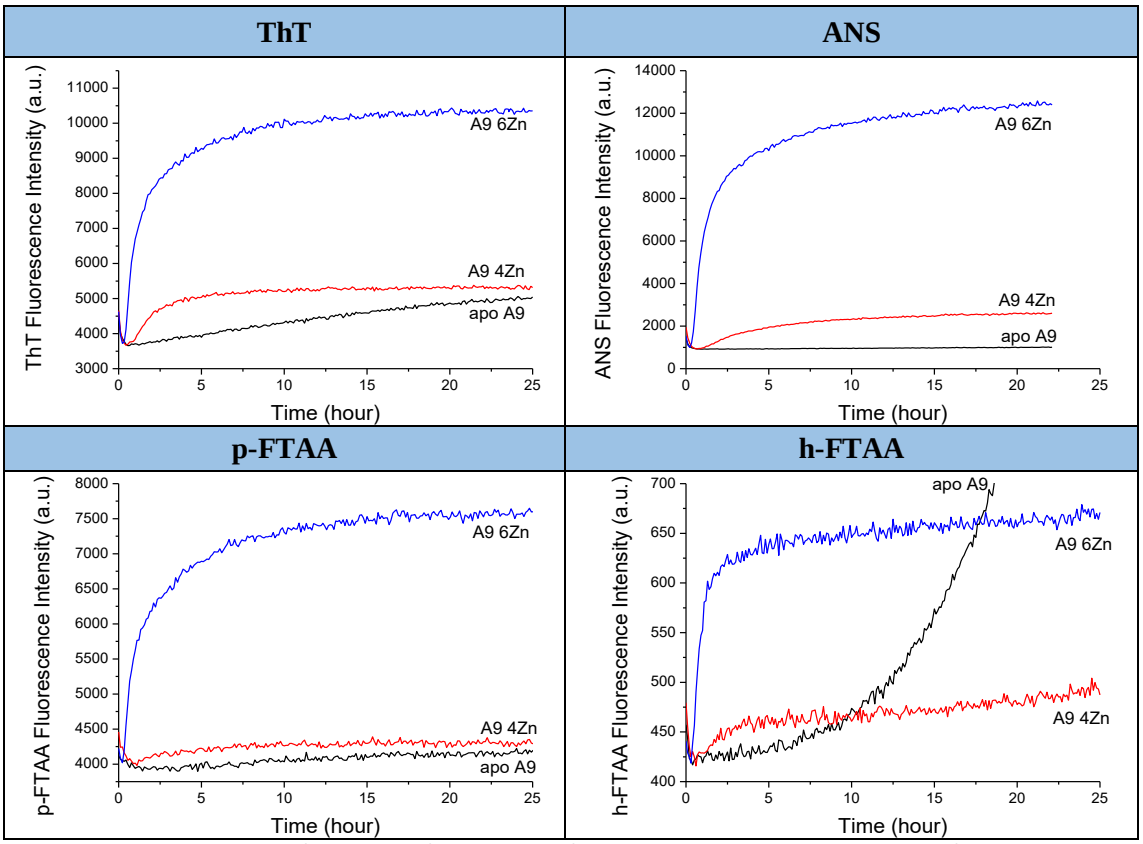

Figure 3.2.9 – Comparison of kinetic profiles obtained for S100A9 alone, 4:1 and 6:1 ratio of Zn/S100A9, with different probes.

Comparing the kinetic profile obtained with each probe for the apo S100A9, it is possible to observe that, in absence of divalent metal ions, the conformational changes that occurred did not result in the formation of amyloid structures, since no significant fluorescence was observed (for ThT, ANS and p-FTAA). ThT reactivity suggests a slow increasing of ThT-reactive species and in small quantities. On the other hand, ANS binding did not occur, meaning that there was no hydrophobic regions exposed, during the incubation period. Regarding p-FTAA and h-FTAA, they showed contradictory effects, which was rather surprising given that both are expected to interact with same type of species, however this interaction is known to occur differently. For this reason, it is possible that h-FTAA is able to detect species that p-FTAA cannot. Overall, none of this probes seemed to be the best fit to report what is happening to apo S100A9, however we could exclude the possibility of amyloids formation.

Regarding the effect of Zn^{2+} on S100A9 aggregation, all probes exhibited reactivity, indicating occurrence of a complex self-assembly reaction. For the 4Zn/S100A9 ratio, some differences are visible from each probe. It seems that ThT-positive species are being formed faster than the supposed intermediates detected by LCOs. Moreover, the formation of ThT- and non-ThT reactive species appears to be associated with the exposition of hydrophobic regions (reported by ANS), due to major conformational adjustments. However, the h-FTAA profile indicates what it seems to be the occurrence of a second event, starting at ~12h. In situations with higher amounts of zinc, in this case 6Zn/S100A9, reactivity for all probes continues to occur, but with a higher rate (higher slope), fluorescence intensity and shorter lag phase, meaning that this event is, as expect from earlier results, enhanced with increasing amounts of zinc. However, the minor details in the kinetic profiles, reported for the 4:1 ratio, are no longer observable. Overall, the Zn^{2+}-induced S100A9 aggregation reported by ThT was also described by the LCOs and ANS, demonstrating this phenomenon complexity.

3.2.2. Analysis of the formation of Ca-dependent aggregates and the effect combined of Zn and Ca

The abovementioned findings about zinc's ability to induce S100A9 aggregation led us to investigate the possibility of calcium alone or with zinc being also capable of similar effects. As it has been previously described for other S100 proteins, the S100A9 homodimer has four Ca^{2+}-binding sites [108]. Hence, in the following assays we incubated the S100A9 homodimer with Ca^{2+} alone, ranging from 0 to 4-fold protein's concentration, and in combination with Zn^{2+}. We did a Ca^{2+} gradient over a non-aggregating Zn/S100A9 ratio and a Zn^{2+} gradient (0 to 3-fold protein's concentration) over a full Ca^{2+}-loaded S100A9 homodimer to see how these two metals together influence S100A9 self-assembly.

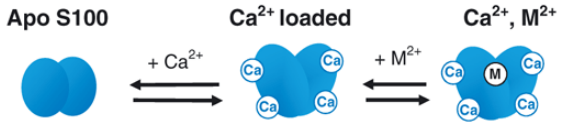

Figure 3.2.10 – Binding of both Ca^{2+} and a transition metal (in our case, Zn^{2+}) to S100 protein.

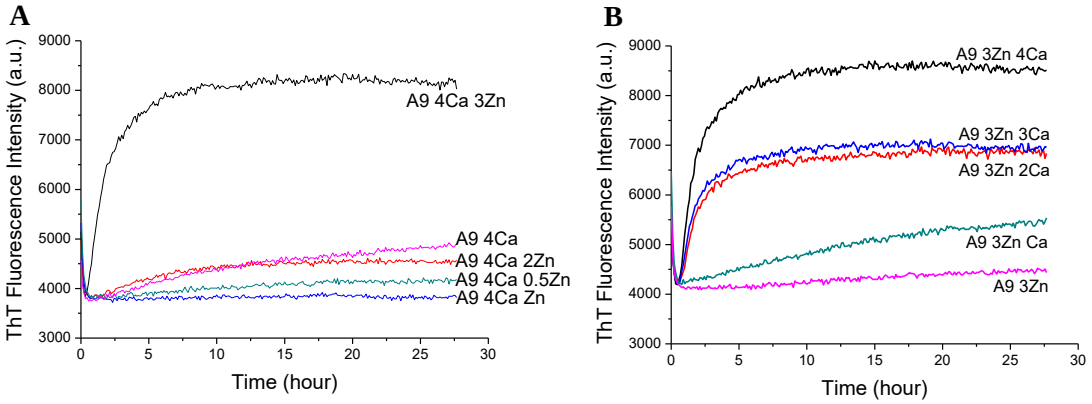

Figure 3.2.11 – Zn^{2+} and Ca^{2+} together induced S100A9 aggregation. (A) Ca^{2+} gradient over a non-aggregator Zn^{2+} concentration. (B) Zn^{2+} gradient over a full Ca^{2+}-loaded S100A9 homodimer.

Since calcium is a natural ligand of S100A9 one should expect that Ca^{2+}-binding would not induce amyloid aggregation of S100A9, which was indeed confirmed by the kinetic data above represented (Figure 3.2.11), where low ThT reactivity was observed when Ca^{2+} was present at 4:1 ratio of Ca/S100A9 (pink curve in panel A). Surprisingly, increasing concentrations of Ca^{2+} induced S100A9 aggregation when loaded with non-aggregating Zn concentration (panel B) and vice versa (panel A). Furthermore, the sample, similarly to 4Zn/S100A9 condition, became turbid and formed a precipitate.

Overall, the data above demonstrated an additive effect, where the formation of ThT-reactive species was induced by concomitant addition of Ca^{2+} and Zn^{2+} to S100A9 at specific concentrations.

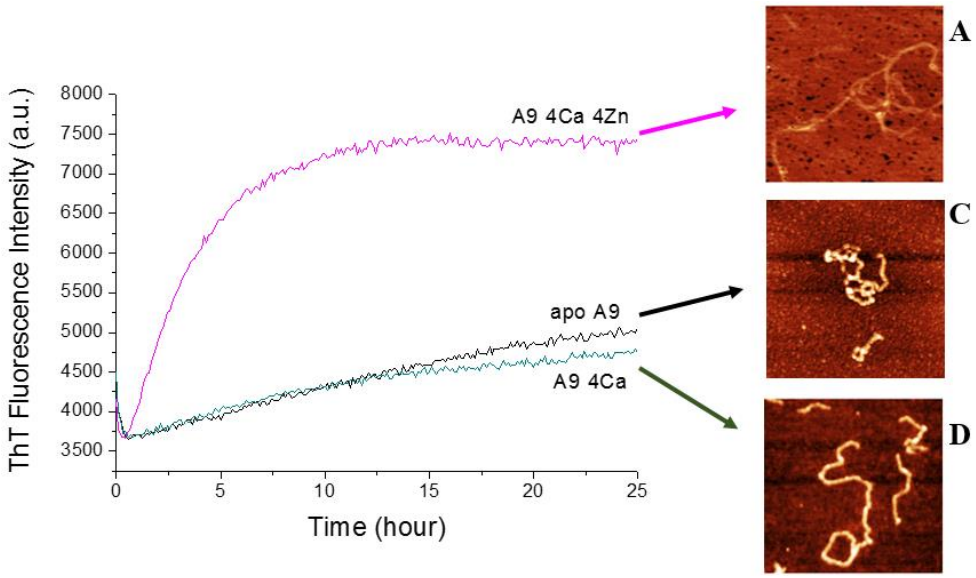

Figure 3.2.12 – Correlation between ThT kinetics and AFM imaging of S100A9 4Ca samples incubated 25h at 37ºC with 250rpm agitation. Images with different scan sizes: (A) 2 µm, (B) and (C) 1 µm

As it is depicted in Figure 3.2.12, the presence of 4Ca induced the formation of string-like structures similar to the ones obtained for S100A9 alone, however these ones were bigger with a length of 439 ± 32 nm. Since Ca^{2+} is considered to be a natural ligand of S100A9 and the aggregation assays did not show amyloid-like behaviour, therefore we put forward the possibility that these structures can be some kind of functional aggregates. Considering the results for the apo S100A9, it is possible to hypothesize that this features can be formed by S100A9 alone and that Ca^{2+} may have a role in accelerating this process. Additionally, images from 5, 15, 25 hours showed a polymerization reaction (Figure 3.2.13).

The concomitant addition of $4Ca^{2+}$ and $4Zn^{2+}$ to S100A9 lead to formation of a wide range of fibril-like structures and also some amorphous aggregates. The presence of the two metals could be the key to produce amyloid fibrils. This hypothesis has already been proposed for S100A8/A9 [115].

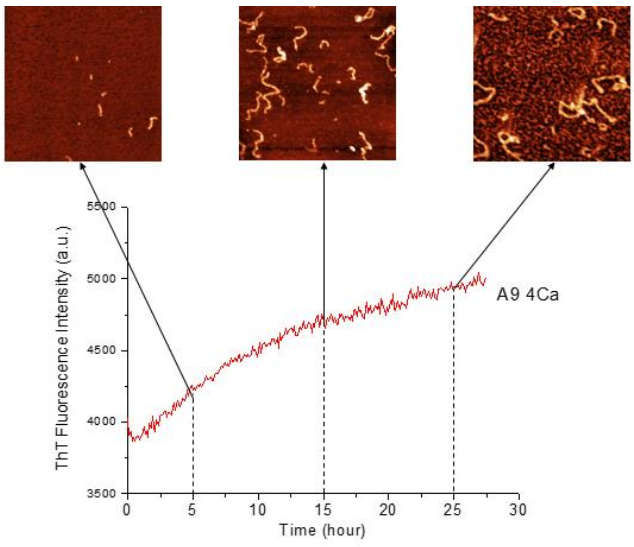

Figure 3.2.13 – AFM imaging shows polymerization reaction induced by Ca^{2+}. Images taken at 5, 15 and 25 hours of incubation.

We then tested the effect of EDTA on these metal-induced structures to see if it could revert to its initial state.

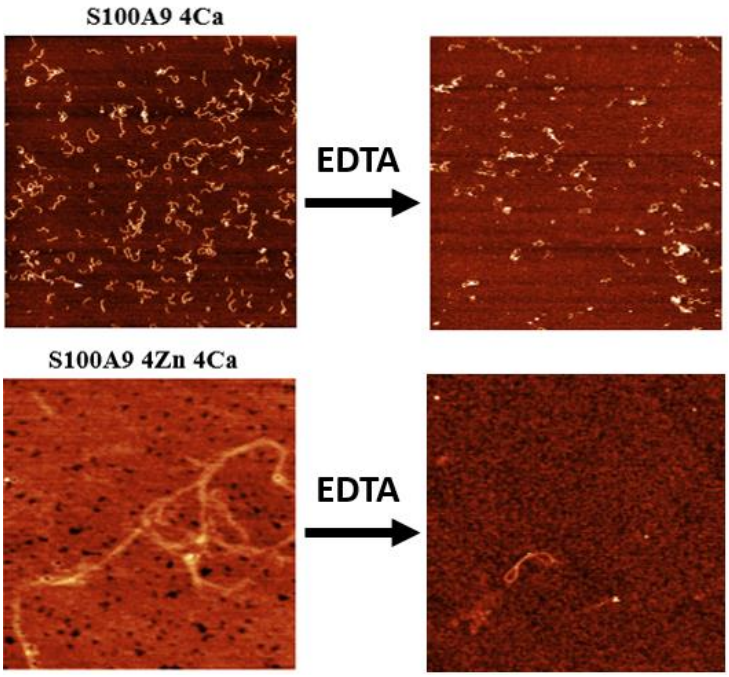

Figure 3.2.14 – AFM imaging of EDTA effect on metal-dependent S100A9 structures.

Interestingly, the amount of Ca^{2+}-induced strings was lower after addition of EDTA, as well as their length, becoming more similar to the ones formed by the apo S100A9. Statistics showed that their length went decreased from 439 ± 32 nm to 268 ± 18 nm. Lastly, the fibrils observed in S100A9 4Zn 4Ca condition disappeared or became smaller. Overall, the EDTA effect showed that without metals these assemblies become less stable, therefore leading to some degree of dissociation.

Afterwards, similarly to what was performed for Zn^{2+} effect on S100A9, the same probes were used to further analyze the conformational changes induced by Ca^{2+} alone and with Zn^{2+}.

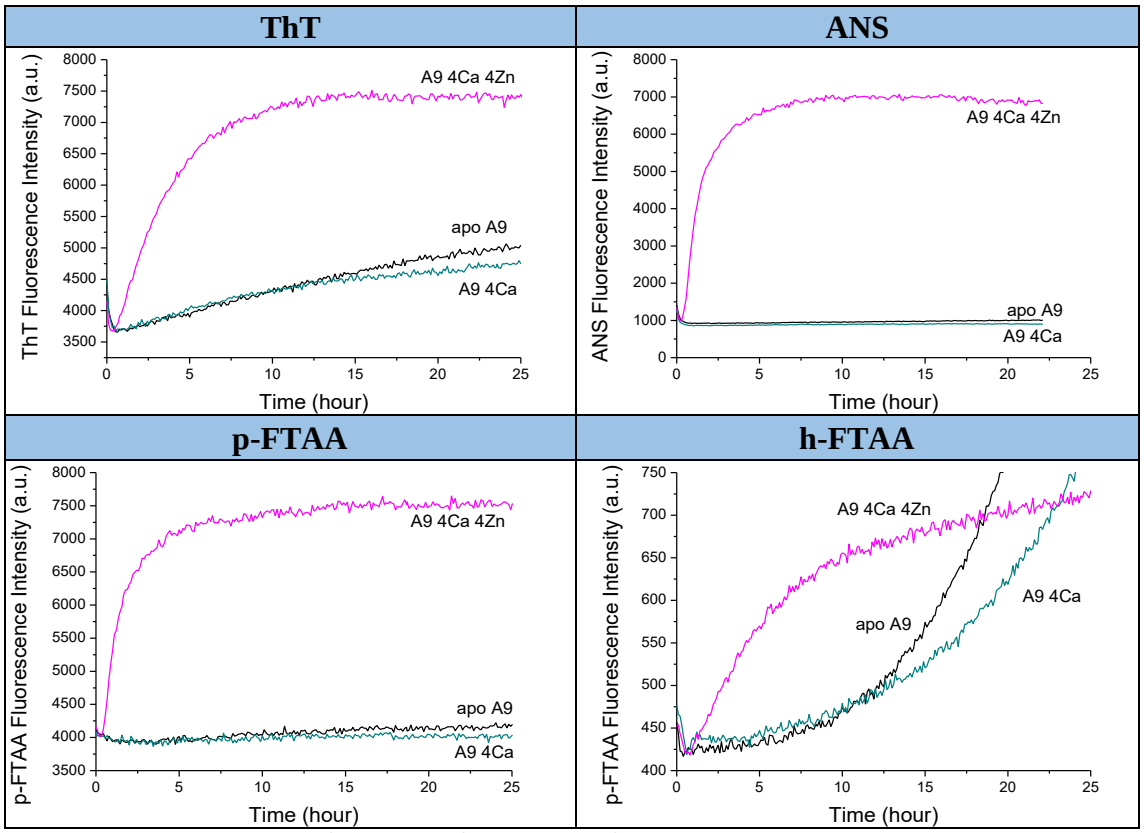

Figure 3.2.15 - Comparison of kinetic profiles obtained for S100A9 alone, 4:1 Ca/S100A9 ratio and 4:4:1 Ca/Zn/S100A9 ratio, with different probes.

The interaction between S100A9 and $4Ca^{2+}$, revealed similar kinetic profiles, for each probe, to the ones of apo S100A9, suggesting that the similar conformational changes are happening. Interestingly, the combined effect of $4Zn^{2+}$ and $4Ca^{2+}$ on S100A9 was reported by all probes. However the results suggest a distinct aggregation pathway from the other conditions. In this case, ANS and p-FTAA reactivity appeared to be superimposable, suggesting formation of intermediate species with exposure of the protein's hydrophobic patches, and later ThT reactivity suggests formation of amyloid structures, possibly fibrils (seen in Figure 3.2.12 A). On the other hand, h-FTAA showed that non-ThT reactive species were formed in a mid-stage of the recorded process, contributing to complexity of this self-assembly.

Overall, the 25 hour incubation of S100A9 with Ca^{2+} occurred in a very similar way than the apo S100A9. Although these probes were incapable of describing the conformational changes induced by Ca^{2+}, it is possible to assume that this phenomenon is greatly distinct from the other conditions. Regarding S100A9 binding to both Zn^{2+} and Ca^{2+}, a complex aggregation occurred with formation of amyloid-like structures.

3.2.3. Imunodetection and SEC analysis discriminate metal-induced structures

To further characterize the S100A9 aggregates in the presence of the studied metal ions, conformation-dependent antibodies that specifically recognize polypeptide chains with a given conformation, were used. The antibodies used were the OC and A11. The OC antibody is capable of recognizing amyloid fibrils, while the A11 specifically recognizes to prefibrillar oligomers [147, 148]. Different dilutions of the S100A9 samples were tested to assess which condition retrieved a stronger reaction with the antibody.

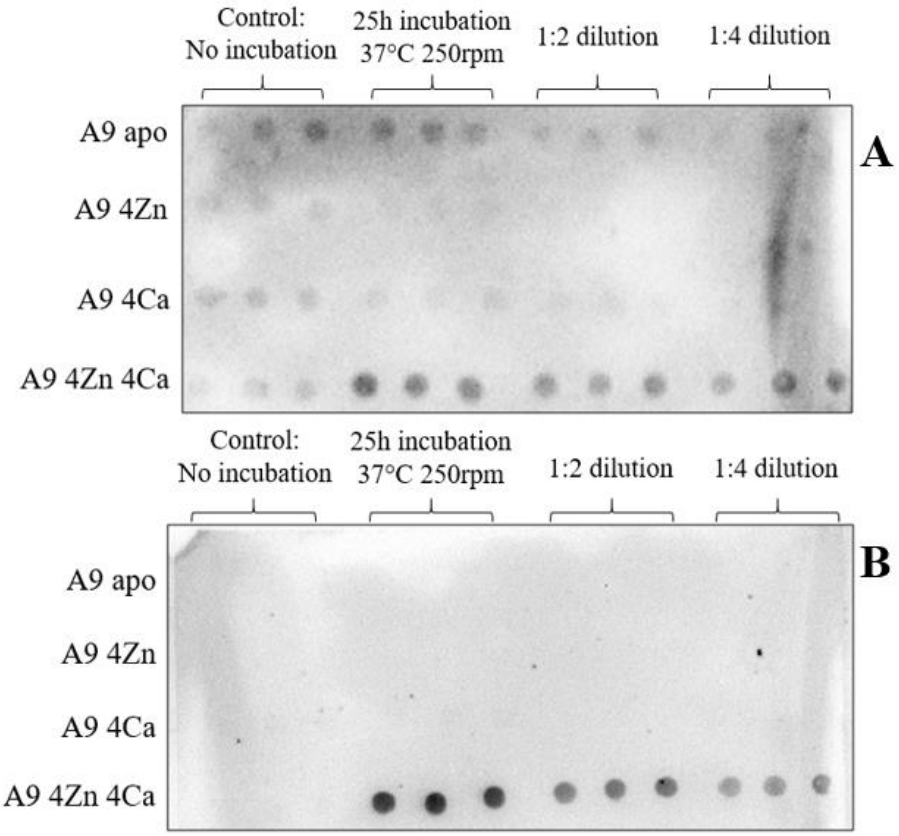

Figure 3.2.16 – Dotblot of the 25h end-points of metal-induced aggregates. (A) OC reactivity to amyloid fibrils (B) A11 reactivity to prefibrillar oligomers.

This experiment (Figure 3.2.16) revealed that the incubation of S100A9 with $4Zn^{2+}$ and $4Ca^{2+}$ resulted in formation of species reactive to both antibodies, suggesting therefore the presence of amyloid fibrils and also prefibrillar oligomers. On the other hand, for the other conditions reaction to A11 was not observed, thus excluding the possibility of existence of prefibrillar oligomers. However, low reactivity to OC antibody was observed, which should mean presence of amyloid fibrils, but when compared to non-incubated S100A9 for all conditions, it is not possible be sure that amyloid fibrils cause this immunoreactivity.

Next, we used another approach to assess protein conformational changes by passing proteins through a size exclusion chromatography (SEC). This method allows monitoring of protein size changes using the column's calibration curve (Figure 2.2.1), however assuming its globular state. The samples were injected in the column after 25 hour incubation at 37 ºC and agitation. Moreover the effect of EDTA was also analyzed. The results obtained showed present of only one peak for each samples with molecular masses ranging 31-49 kDa (Figure 3.2.17).

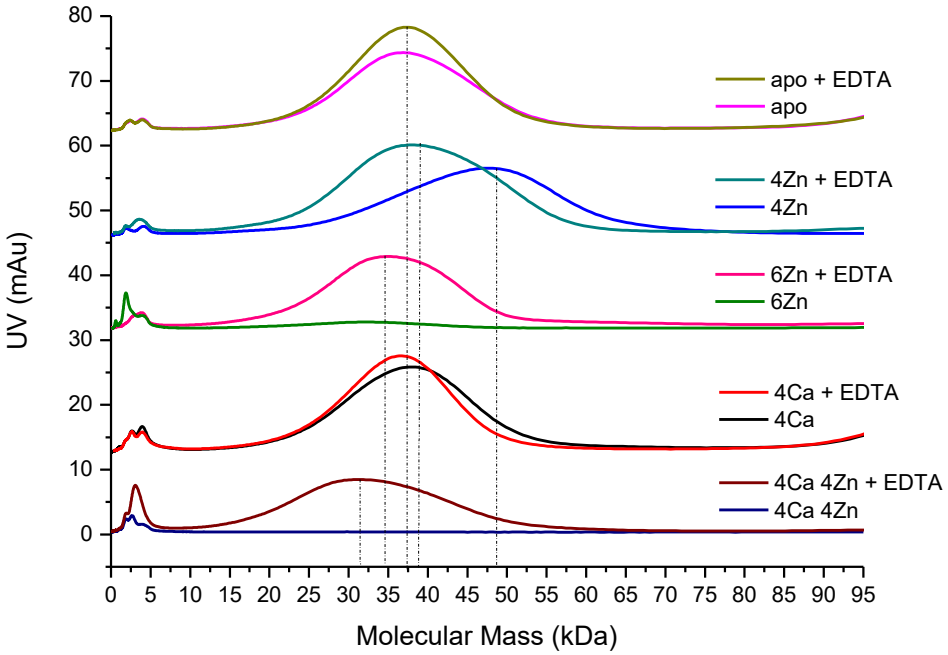

Figure 3.2.17 – Aggregation analysis by SEC reveals S100A9 species with different sizes.

As it can be observed above, the chromatograms that represent the apo S100A9 and 4Ca/S100A9 conditions are very similar, with an insignificant difference of ~2 kDa, which is in accordance with the similarity described in the experiments discussed earlier. In this conditions, the peak displayed a molecular mass of ~37 and ~39 kDa which is larger than the S100A9 homodimer but smaller then tetramer, meaning that the homodimer could be in a more relaxed conformation rather than the classic globular shape, thus appearing larger.

On the other hand, the chromatogram of 4Zn/S100A9 showed a peak with maximum size of ~49 kDa, suggesting formation of S100A9 tetramer, which could be possible considering the findings reported in the literature [109] and also the AFM data.

The analysis of S100A9 in presence of Zn^{2+} at a 6:1 ratio and in presence of both Zn^{2+} and Ca^{2+} was impossible to performed, because of the large amount of precipitate that could not be loaded into the column.

Here, the EDTA did not produce any significant change on apo S100A9 and 4Ca/S100A9's chromatogram, however for the other conditions the effect was very interesting. After EDTA addition, 4Zn/S100A9 presented a shift of peak to a lower molecular mass, suggesting dissociation of tetramer into dimer. Lastly, the recovery of the insoluble protein correlated with the arising of a peak, demonstrating once more, the metal dependence of this assemblies. Figure 3.2.18 represents how the quantity of soluble protein is altered by metal binding and addition of EDTA.

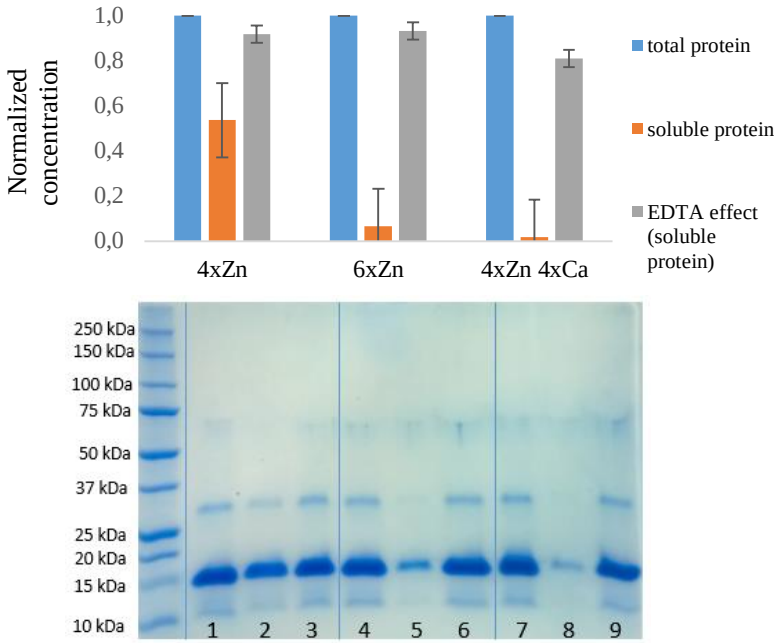

Figure 3.2.18 – Changes in quantities of soluble protein induced by metal binding and EDTA. (A) Bar chart representing bradford quantification. (B) SDS-PAGE of the respective conditions in chart above.

IV. Conclusions

Protein misfolding and aggregation events are known to be associated with a variety of human disorders, such as Alzheimer's disease (AD) [140]. In the context of AD, the S100A9 protein has been proposed to participate as potent pro-inflammatory protein and by forming amyloid aggregates, which co-aggregate with Aβ peptide, thus increasing the pathologic state of the disease [150]. Considering that S100A9 is a Ca^{2+} and Zn^{2+}-binding protein and that metals are capable of inducing conformational changes [82], one would expect that the interaction of S100A9 with these metals could be the source of amyloid aggregation and the cytotoxicity that arises with it.

In this study we have demonstrated an effect of Zn^{2+} over S100A9 aggregation when present in concentrations above its binding capacity [108]. This interaction led to the formation of ThT-reactive species but only when S100A9 concentration was above 10μM (critical concentration to aggregate). Moreover, increasing concentrations of S100A9 or Zn^{2+} lead to faster aggregation, which presented visually as a white turbid precipitate. The possibility of this aggregation could be driven by an electrostatic effect was ruled out by ThT kinetics of S100A9 with excess of NaCl, since it did not reproduce same effect as Zn^{2+}. The results for other aggregation probes are in agreement with the existence of this aggregation phenomenon. Furthermore, seeding experiments did not show amyloid-like behaviour, as well AFM imaging and imunodetection with OC and A11 antibodies did not display presence of amyloid fibrils, but instead this aggregates appeared as individual globular features. Overall, this findings suggest that S100A9 forms non-amyloid aggregates which precipitate with a possible role in Zn^{2+} chelation.

Regarding the role of Ca^{2+}, its effect was hardly reported by the probes used, excluding the formation of amyloid-like structures. Indeed this hypothesis was confirmed by the results from immunoreactivity of OC and A11 antibodies who showed no detection. Interestingly, AFM imaging assays showed the formation of string-like structures, carried out through a polymerization reaction. Hence, we demonstrated that Ca^{2+} is capable of inducing the formation of "aggregates", however these may have a biological function, rather than a toxic effect.

When combined together Zn^{2+} and Ca^{2+} produced an additive effect that was displayed by the binding of the different aggregation reporters, probes and antibodies. Also, the AFM imaging showed presence of fibrils in these samples, confirming that the interaction of S100A9 with these metals leads to formation of amyloidogenic structures.

Furthermore, we have demonstrated that the assemblies formed are highly dependent on metals, as EDTA was capable of disrupting them, differently. Amazingly, EDTA was able to recover almost all insoluble protein to a soluble state.

Altogether, the results from this work contribute to unveil possible mechanisms through which Zn^{2+} and Ca^{2+} binding influences S100A9 self-assembly reaction and will open new avenues for investigations on the roles of such assemblies in pathophysiological conditions.

In a near future it would be interesting to further characterize the formed species using circular dichroism, a technique which would allow us to unveil the alterations in the protein's secondary structure upon metal binding. Furthermore, it would be of great importance to study the possible toxicity of each of the species formed in each condition, as to shed light in the relevance of S100A9's interaction with Zn^{2+} and Ca^{2+} to the onset of the disease. Finally, we are currently using a promising approach which is AFM imaging in solution in order to record the whole conformational process induced by Ca^{2+} and Zn^{2+} on S100A9.

V. Bibliography

1. Balchin, D., M. Hayer-Hartl, and F.U. Hartl, *In vivo aspects of protein folding and quality control.* Science, 2016. 353(6294): p. aac4354.
2. Dobson, C.M., *The structural basis of protein folding and its links with human disease.* Philos Trans R Soc Lond B Biol Sci, 2001. 356(1406): p. 133-45.
3. Dobson, C.M., *Protein folding and misfolding.* Nature, 2003. 426(6968): p. 884-90.
4. Horwich, A., *Protein aggregation in disease: a role for folding intermediates forming specific multimeric interactions*, in *J Clin Invest*. 2002. p. 1221-32.
5. Tan, S.Y. and M.B. Pepys, *Amyloidosis.* Histopathology, 1994. 25(5): p. 403-14.
6. Kelly, J.W., *The alternative conformations of amyloidogenic proteins and their multi-step assembly pathways.* Curr Opin Struct Biol, 1998. 8(1): p. 101-6.
7. Dobson, C.M., *Protein Misfolding, Aggregation, and Conformational Diseases*, ed. A.L.F. Vladimir N. Uversky. Vol. 4. 2016: SpringerSBM.
8. Leal, S.S., H.M. Botelho, and C.M. Gomes, *Metal ions as modulators of protein conformation and misfolding in neurodegeneration.* Coordination Chemistry Reviews, 2012. 256(19-20): p. 2253-2270.
9. Amit Kessel, N.B.-T., *Protein Structure*, in *Introduction to Proteins: Structure, Function, and Motion*2010: CRC Press. p. 654.
10. Brooks, C.L., 3rd, J.N. Onuchic, and D.J. Wales, *Statistical thermodynamics. Taking a walk on a landscape.* Science, 2001. 293(5530): p. 612-3.
11. Hardesty, B. and G. Kramer, *Folding of a nascent peptide on the ribosome.* Prog Nucleic Acid Res Mol Biol, 2000. 66: p. 41-66.
12. Bukau, B. and A.L. Horwich, *The Hsp70 and Hsp60 chaperone machines.* Cell, 1998. 92(3): p. 351-66.
13. Hartl, F.U. and M. Hayer-Hartl, *Molecular chaperones in the cytosol: from nascent chain to folded protein.* Science, 2002. 295(5561): p. 1852-8.
14. Ellis, R.J., *Macromolecular crowding: an important but neglected aspect of the intracellular environment.* Curr Opin Struct Biol, 2001. 11(1): p. 114-9.
15. Gething, M.J. and J. Sambrook, *Protein folding in the cell.* Nature, 1992. 355(6355): p. 33-45.
16. Ellis, R.J. and F.U. Hartl, *Principles of protein folding in the cellular environment.* Curr Opin Struct Biol, 1999. 9(1): p. 102-10.
17. Schiene, C. and G. Fischer, *Enzymes that catalyse the restructuring of proteins.* Curr Opin Struct Biol, 2000. 10(1): p. 40-5.
18. Hammond, C. and A. Helenius, *Quality control in the secretory pathway.* Curr Opin Cell Biol, 1995. 7(4): p. 523-9.
19. Kaufman, R.J., et al., *The unfolded protein response in nutrient sensing and differentiation.* Nat Rev Mol Cell Biol, 2002. 3(6): p. 411-21.
20. Bennink, U.S., et al., *Rapid degradation of a large fraction of newly synthesized proteins byproteasomes.* Nature, 2000. 404(6779): p. 770-774.
21. Bence, N.F., R.M. Sampat, and R.R. Kopito, *Impairment of the ubiquitin-proteasome system by protein aggregation.* Science, 2001. 292(5521): p. 1552-5.
22. J. Fraústo da Silva, R.W., *The Biological Chemistry of the Elements*. 1991, Oxford: Oxford University Press.
23. Permiakov, E.A., *Metalloproteomics*. 2016, Hoboken, NJ: John Wiley & Sons.
24. Cláudio M. Gomes, P.W.-S., *Protein Folding and Metal Ions: Mechanisms, Biology and Disease*. 2010, Boca Raton: CRC Press. 308.
25. Wittung-Stafshede*, I.P.a. and Pernilla, *Biological Relevance of Metal Binding before Protein Folding.* 2001.
26. Leckner, J., et al., *The effect of the metal ion on the folding energetics of azurin: a comparison of the native, zinc and apoprotein.* Biochim Biophys Acta, 1997. 1342(1): p. 19-27.
27. Tottey, S., D.R. Harvie, and N.J. Robinson, *Understanding how cells allocate metals using metal sensors and metallochaperones.* Acc Chem Res, 2005. 38(10): p. 775-83.
28. Dobson, C.M., *Protein folding and disease: a view from the first Horizon Symposium*, in *Nat Rev Drug Discov*. 2003: England. p. 154-60.
29. Macario, A.J. and E. Conway de Macario, *Sick chaperones and ageing: a perspective.* Ageing Res Rev, 2002. 1(2): p. 295-311.
30. Hardy, J. and D.J. Selkoe, *The amyloid hypothesis of Alzheimer's disease: progress and problems on the road to therapeutics.* Science, 2002. 297(5580): p. 353-6.
31. Haass, C. and D.J. Selkoe, *Soluble protein oligomers in neurodegeneration: lessons from the Alzheimer's amyloid beta-peptide.* Nat Rev Mol Cell Biol, 2007. 8(2): p. 101-12.
32. Spillantini, M.G., et al., *Alpha-synuclein in Lewy bodies.* Nature, 1997. 388(6645): p. 839-40.
33. Polymeropoulos, M.H., et al., *Mutation in the alpha-synuclein gene identified in families with Parkinson's disease.* Science, 1997. 276(5321): p. 2045-7.
34. Saibil, J.L.J., et al., *The protofilament structure of insulin amyloid fibrils*. 2002.
35. Sunde, M., et al., *Common core structure of amyloid fibrils by synchrotron X-ray diffraction.* J Mol Biol, 1997. 273(3): p. 729-39.
36. Müller, A., et al., *Atomic structure and hierarchical assembly of a cross-β amyloid fibril.* 2013.
37. Dobson, C.M., *Protein misfolding, evolution and disease.* Trends Biochem Sci, 1999. 24(9): p. 329-32.
38. Fandrich, M. and C.M. Dobson, *The behaviour of polyamino acids reveals an inverse side chain effect in amyloid structure formation.* Embo j, 2002. 21(21): p. 5682-90.
39. Chiti, F., et al., *Rationalization of the effects of mutations on peptide and protein aggregation rates.* Nature, 2003. 424(6950): p. 805-8.
40. Meehan, et al., *Metastability of Native Proteins and the Phenomenon of Amyloid Formation.* 2011.
41. Gazit, E., *The "Correctly Folded" state of proteins: is it a metastable state?* Angew Chem Int Ed Engl, 2002. 41(2): p. 257-9.
42. Knowles, T.P., M. Vendruscolo, and C.M. Dobson, *The amyloid state and its association with protein misfolding diseases.* Nat Rev Mol Cell Biol, 2014. 15(6): p. 384-96.
43. Tartaglia, G.G., et al., *Life on the edge: a link between gene expression levels and aggregation rates of human proteins.* Trends Biochem Sci, 2007. 32(5): p. 204-6.
44. Caughey, B. and P.T. Lansbury, *Protofibrils, pores, fibrils, and neurodegeneration: separating the responsible protein aggregates from the innocent bystanders.* Annu Rev Neurosci, 2003. 26: p. 267-98.

45. Bitan, G., et al., *Amyloid β-protein (Aβ) assembly: Aβ40 and Aβ42 oligomerize through distinct pathways*, in *Proc Natl Acad Sci U S A*. 2003. p. 330-5.
46. Schlunegger, M.P., M.J. Bennett, and D. Eisenberg, *Oligomer formation by 3D domain swapping: a model for protein assembly and misassembly.* Adv Protein Chem, 1997. 50: p. 61-122.
47. Tanaka, M., et al., *The physical basis of how prion conformations determine strain phenotypes.* Nature, 2006. 442(7102): p. 585-9.
48. Jucker, M. and L.C. Walker, *Pathogenic protein seeding in Alzheimer disease and other neurodegenerative disorders.* Ann Neurol, 2011. 70(4): p. 532-40.
49. Knowles, S.I.A.C., et al., *Proliferation of amyloid-β42 aggregates occurs through a secondary nucleation mechanism.* 2013.
50. Knowles, T.P., et al., *An analytical solution to the kinetics of breakable filament assembly.* Science, 2009. 326(5959): p. 1533-7.
51. Eisenberg, D. and M. Jucker, *The amyloid state of proteins in human diseases.* Cell, 2012. 148(6): p. 1188-203.
52. Chiti, F. and C.M. Dobson, *Protein misfolding, functional amyloid, and human disease.* Annu Rev Biochem, 2006. 75: p. 333-66.
53. Cremades, N., et al., *Direct observation of the interconversion of normal and toxic forms of alpha-synuclein.* Cell, 2012. 149(5): p. 1048-59.
54. Walsh, D.M., et al., *Naturally secreted oligomers of amyloid beta protein potently inhibit hippocampal long-term potentiation in vivo.* Nature, 2002. 416(6880): p. 535-9.
55. Lesne, S., et al., *A specific amyloid-beta protein assembly in the brain impairs memory.* Nature, 2006. 440(7082): p. 352-7.
56. Stefani, M.B., et al., *Inherent toxicity of aggregates implies a common mechanism for protein misfolding diseases.* Nature, 2002. 416(6880): p. 507-511.
57. Billings, L.M., et al., *Intraneuronal Abeta causes the onset of early Alzheimer's disease-related cognitive deficits in transgenic mice.* Neuron, 2005. 45(5): p. 675-88.
58. Tartaglia, G.G., et al., *Prediction of aggregation-prone regions in structured proteins.* J Mol Biol, 2008. 380(2): p. 425-36.
59. Broome, B.M. and M.H. Hecht, *Nature disfavors sequences of alternating polar and non-polar amino acids: implications for amyloidogenesis.* J Mol Biol, 2000. 296(4): p. 961-8.
60. Otzen, D.E. and M. Oliveberg, *Salt-induced detour through compact regions of the protein folding landscape.* Proc Natl Acad Sci U S A, 1999. 96(21): p. 11746-51.
61. Webb, J.L., et al., *Alpha-Synuclein is degraded by both autophagy and the proteasome.* J Biol Chem, 2003. 278(27): p. 25009-13.
62. Rubinsztein, D.C., *The roles of intracellular protein-degradation pathways in neurodegeneration.* Nature, 2006. 443(7113): p. 780-6.
63. Mizushima, N., et al., *Autophagy fights disease through cellular self-digestion.* Nature, 2008. 451(7182): p. 1069-75.
64. Marenholz, I., C.W. Heizmann, and G. Fritz, *S100 proteins in mouse and man: from evolution to function and pathology (including an update of the nomenclature).* Biochem Biophys Res Commun, 2004. 322(4): p. 1111-22.
65. Moore, B.W., *A soluble protein characteristic of the nervous system.* Biochem Biophys Res Commun, 1965. 19(6): p. 739-44.
66. Donato, R., *S100: a multigenic family of calcium-modulated proteins of the EF-hand type with intracellular and extracellular functional roles.* Int J Biochem Cell Biol, 2001. 33(7): p. 637-68.
67. Donato, R., *RAGE: a single receptor for several ligands and different cellular responses: the case of certain S100 proteins.* Curr Mol Med, 2008. 7(8): p. 711-24.
68. Chen, M., et al., *Integrin alpha6beta4 controls the expression of genes associated with cell motility, invasion, and metastasis, including S100A4/metastasin.* J Biol Chem, 2008. 284(3): p. 1484-94.
69. Donato, R., et al., *S100B's double life: intracellular regulator and extracellular signal.* Biochim Biophys Acta, 2008. 1793(6): p. 1008-22.
70. Ehrchen, J.M., et al., *The endogenous Toll-like receptor 4 agonist S100A8/S100A9 (calprotectin) as innate amplifier of infection, autoimmunity, and cancer.* J Leukoc Biol, 2009. 86(3): p. 557-66.
71. Hsu, K., et al., *ANTI-INFECTIVE PROTECTIVE PROPERTIES OF S100 CALGRANULINS.* Antiinflamm Antiallergy Agents Med Chem, 2010. 8(4): p. 290-305.
72. Eggers, K., et al., *RAGE-dependent regulation of calcium-binding proteins S100A8 and S100A9 in human THP-1.* Exp Clin Endocrinol Diabetes, 2011. 119(6): p. 353-7.
73. Salama, I., et al., *A review of the S100 proteins in cancer.* Eur J Surg Oncol, 2007. 34(4): p. 357-64.
74. Mori, T., et al., *Overexpression of human S100B exacerbates cerebral amyloidosis and gliosis in the Tg2576 mouse model of Alzheimer's disease.* Glia, 2009. 58(3): p. 300-14.
75. Peskind, E.R., et al., *Cerebrospinal fluid S100B is elevated in the earlier stages of Alzheimer's disease.* Neurochem Int, 2001. 39(5-6): p. 409-13.
76. Boom, A., et al., *Astrocytic calcium/zinc binding protein S100A6 over expression in Alzheimer's disease and in PS1/APP transgenic mice models.* Biochim Biophys Acta, 2004. 1742(1-3): p. 161-8.
77. Mrak, R.E. and W.S. Griffinbc, *The role of activated astrocytes and of the neurotrophic cytokine S100B in the pathogenesis of Alzheimer's disease.* Neurobiol Aging, 2002. 22(6): p. 915-22.
78. Foell, D. and J. Roth, *Proinflammatory S100 proteins in arthritis and autoimmune disease.* Arthritis Rheum, 2004. 50(12): p. 3762-71.
79. Schafer, B.W. and C.W. Heizmann, *The S100 family of EF-hand calcium-binding proteins: functions and pathology.* Trends Biochem Sci, 1996. 21(4): p. 134-40.
80. Bunick, C.G., et al., *Designing sequence to control protein function in an EF-hand protein.* J Am Chem Soc, 2004. 126(19): p. 5990-8.
81. Nacken, C.P., et al., *Analysis of the MRP8-MRP14 Protein-Protein Interaction by the Two-hybrid System Suggests a Prominent Role of the C-terminal Domain of S100 Proteins in Dimer Formation.* 1999.
82. Gilston, B.A., E.P. Skaar, and W.J. Chazin, *Binding of transition metals to S100 proteins.* Sci China Life Sci, 2016. 59(8): p. 792-801.
83. Fritz, G., et al., *Natural and amyloid self-assembly of S100 proteins: structural basis of functional diversity.* The FEBS Journal, 2016. 277(22): p. 4578-4590.

84. Ostendorp, T., et al., *Structural and functional insights into RAGE activation by multimeric S100B.* EMBO J, 2007. 26(16): p. 3868-78.
85. Koch, M., et al., *Implications on zinc binding to S100A2.* Biochim Biophys Acta, 2007. 1773(3): p. 457-70.
86. Korndorfer, I.P., F. Brueckner, and A. Skerra, *The crystal structure of the human (S100A8/S100A9)2 heterotetramer, calprotectin, illustrates how conformational changes of interacting alpha-helices can determine specific association of two EF-hand proteins.* J Mol Biol, 2007. 370(5): p. 887-98.
87. Moroz, O.V., et al., *The crystal structures of human S100A12 in apo form and in complex with zinc: new insights into S100A12 oligomerisation.* J Mol Biol, 2009. 391(3): p. 536-51.
88. Moroz, O.V., et al., *The structure of S100A12 in a hexameric form and its proposed role in receptor signalling.* Acta Crystallogr D Biol Crystallogr, 2002. 58(Pt 3): p. 407-13.
89. Donato, R., et al., *Functions of S100 proteins.* Curr Mol Med, 2012. 13(1): p. 24-57.
90. Carvalho, S.B., et al., *Intrinsically disordered and aggregation prone regions underlie beta-aggregation in S100 proteins.* PLoS One, 2013. 8(10): p. e76629.
91. Yanamandra, K., et al., *Amyloid formation by the pro-inflammatory S100A8/A9 proteins in the ageing prostate.* PLoS One, 2009. 4(5): p. e5562.
92. Permyakov, S.E., et al., *Intrinsic disorder in S100 proteins.* Mol Biosyst, 2011. 7(7): p. 2164-80.
93. Strynadka, N.C. and M.N. James, *Crystal structures of the helix-loop-helix calcium-binding proteins.* Annu Rev Biochem, 1989. 58: p. 951-98.
94. Kligman, D. and D.C. Hilt, *The S100 protein family.* Trends Biochem Sci, 1988. 13(11): p. 437-43.
95. Maler, L., M. Sastry, and W.J. Chazin, *A structural basis for S100 protein specificity derived from comparative analysis of apo and Ca(2+)-calcyclin.* J Mol Biol, 2002. 317(2): p. 279-90.
96. Nelson, M.R. and W.J. Chazin, *Structures of EF-hand Ca(2+)-binding proteins: diversity in the organization, packing and response to Ca2+ binding.* Biometals, 1999. 11(4): p. 297-318.
97. Nelson, M.R., et al., *The EF-hand domain: A globally cooperative structural unit*, in *Protein Sci*. 2002. p. 198-205.
98. Bhattacharya, S., C.G. Bunick, and W.J. Chazin, *Target selectivity in EF-hand calcium binding proteins.* Biochim Biophys Acta, 2004. 1742(1-3): p. 69-79.
99. Heizmann, C.W. and J.A. Cox, *New perspectives on S100 proteins: a multi-functional Ca(2+)-, Zn(2+)- and Cu(2+)-binding protein family.* Biometals, 1999. 11(4): p. 383-97.
100. Baudier, J., et al., *Purification, characterization and ion binding properties of human brain S100b protein.* Biochim Biophys Acta, 1984. 790(2): p. 164-73.
101. Brodersen, D.E., a. J. Nyborg, and M. Kjeldgaard*, *Zinc-Binding Site of an S100 Protein Revealed. Two Crystal Structures of Ca2+-Bound Human Psoriasin (S100A7) in the Zn2+-Loaded and Zn2+-Free States†,‡.* 1999.
102. Moroz, O.V., K.S. Wilson, and I.B. Bronstein, *The role of zinc in the S100 proteins: insights from the X-ray structures.* Amino Acids, 2010. 41(4): p. 761-72.
103. Schafer, B.W., et al., *Brain S100A5 is a novel calcium-, zinc-, and copper ion-binding protein of the EF-hand superfamily.* J Biol Chem, 2000. 275(39): p. 30623-30.
104. Vogl, T., et al., *Alarmin S100A8/S100A9 as a biomarker for molecular imaging of local inflammatory activity.* Nat Commun, 2014. 5: p. 4593.
105. Roth, J., et al., *Phagocyte-specific S100 proteins: a novel group of proinflammatory molecules.* Trends Immunol, 2003. 24(4): p. 155-8.
106. Edgeworth, J., et al., *Identification of p8,14 as a highly abundant heterodimeric calcium binding protein complex of myeloid cells.* J Biol Chem, 1991. 266(12): p. 7706-13.
107. Teigelkamp, S., et al., *Calcium-dependent complex assembly of the myeloic differentiation proteins MRP-8 and MRP-14.* J Biol Chem, 1991. 266(20): p. 13462-7.
108. Itou, H., et al., *The crystal structure of human MRP14 (S100A9), a Ca(2+)-dependent regulator protein in inflammatory process.* J Mol Biol, 2002. 316(2): p. 265-76.
109. Leukert, N., et al., *Calcium-dependent tetramer formation of S100A8 and S100A9 is essential for biological activity.* J Mol Biol, 2006. 359(4): p. 961-72.
110. Bairoch, A. and R. Apweiler, *The SWISS-PROT protein sequence database and its supplement TrEMBL in 2000.* Nucleic Acids Res, 1999. 28(1): p. 45-8.
111. Sohnle, P.G., et al., *Zinc-reversible antimicrobial activity of recombinant calprotectin (migration inhibitory factor-related proteins 8 and 14).* J Infect Dis, 2000. 182(4): p. 1272-5.
112. Bianchi, M., et al., *Restoration of anti-Aspergillus defense by neutrophil extracellular traps in human chronic granulomatous disease after gene therapy is calprotectin-dependent.* J Allergy Clin Immunol, 2011. 127(5): p. 1243-52.e7.
113. Strupat, K., et al., *Calcium-induced noncovalently linked tetramers of MRP8 and MRP14 are confirmed by electrospray ionization-mass analysis.* J Am Soc Mass Spectrom, 2000. 11(9): p. 780-8.
114. Vogl, T., et al., *Biophysical characterization of S100A8 and S100A9 in the absence and presence of bivalent cations.* Biochim Biophys Acta, 2006. 1763(11): p. 1298-306.
115. Fritz, G., et al., *Natural and amyloid self-assembly of S100 proteins: structural basis of functional diversity*. FEBS J, 2010. 277(22): p. 4578-90.
116. Wilder, P.T., et al., *Solution structure of zinc- and calcium-bound rat S100B as determined by nuclear magnetic resonance spectroscopy.* Biochemistry, 2005. 44(15): p. 5690-702.
117. Ostendorp, T., et al., *The crystal structures of human S100B in the zinc- and calcium-loaded state at three pH values reveal zinc ligand swapping.* Biochim Biophys Acta, 2010. 1813(5): p. 1083-91.
118. Brodersen, D.E., J. Nyborg, and M. Kjeldgaard, *Zinc-binding site of an S100 protein revealed. Two crystal structures of Ca2+-bound human psoriasin (S100A7) in the Zn2+-loaded and Zn2+-free states.* Biochemistry, 1999. 38(6): p. 1695-704.
119. Hoozemans Jj, V.R.R.J.M.E.P., *Neuroinflammation and regeneration in the early stages of Alzheimer's disease pathology*. 2006. 24(Issues 2–3): p. 157–165.
120. Gruden, M.A., et al., *Autoimmune responses to amyloid structures of Abeta(25-35) peptide and human lysozyme in the serum of patients with progressive Alzheimer's disease.* Dement Geriatr Cogn Disord, 2004. 18(2): p. 165-71.
121. Heneka, M.T., et al., *Neuroinflammation in Alzheimer's disease.* Lancet Neurol, 2015. 14(4): p. 388-405.
122. Heneka, M.T. and M.K. O'Banion, *Inflammatory processes in Alzheimer's disease.* J Neuroimmunol, 2007. 184(1-2): p. 69-91.
123. Holmes, C., et al., *Systemic inflammation and disease progression in Alzheimer disease.* Neurology, 2009. 73(10): p. 768-74.

124. Braak, H. and E. Braak, *Neuropathological stageing of Alzheimer-related changes.* Acta Neuropathol, 1991. 82(4): p. 239-59.
125. Crews, L. and E. Masliah, *Molecular mechanisms of neurodegeneration in Alzheimer's disease.* Hum Mol Genet, 2010. 19(R1): p. R12-20.
126. Maynard, C.J., et al., *Metals and amyloid-beta in Alzheimer's disease.* Int J Exp Pathol, 2005. 86(3): p. 147-59.
127. Croce, K., et al., *Myeloid-related protein-8/14 is critical for the biological response to vascular injury.* Circulation, 2009. 120(5): p. 427-36.
128. Shepherd, C.E., et al., *Inflammatory S100A9 and S100A12 proteins in Alzheimer's disease.* Neurobiol Aging, 2005. 27(11): p. 1554-63.
129. Raoul P Kloppenborg, E.R., Marieke ES Sprengers, Dirk Troost, Piet Eikelenboom and Paul J Nederkoorn, *Steroid responsive encephalopathy in cerebral amyloid angiopathy: a case report and review of evidence for immunosuppressive treatment.* Journal of Neuroinflammation, 2010.
130. Rogers, J. and L.F. Lue, *Microglial chemotaxis, activation, and phagocytosis of amyloid beta-peptide as linked phenomena in Alzheimer's disease.* Neurochem Int, 2001. 39(5-6): p. 333-40.
131. Kummer, M.P., et al., *Mrp14 deficiency ameliorates amyloid beta burden by increasing microglial phagocytosis and modulation of amyloid precursor protein processing.* J Neurosci, 2012. 32(49): p. 17824-9.
132. Bogner, S., et al., *Immune activation in amyloid-beta-related angiitis correlates with decreased parenchymal amyloid-beta plaque load.* Neurodegener Dis, 2013. 13(1): p. 38-44.
133. Frenkel, D., et al., *Scara1 deficiency impairs clearance of soluble amyloid-beta by mononuclear phagocytes and accelerates Alzheimer's-like disease progression.* Nat Commun, 2013. 4: p. 2030.
134. Foell, H.W., et al., *MRP8 and MRP14, phagocyte-specific danger signals, are sensitive biomarkers of disease activity in cryopyrin-associated periodic syndromes.* 2011.
135. Sutinen, E.M., et al., *Pro-inflammatory interleukin-18 increases Alzheimer's disease-associated amyloid-beta production in human neuron-like cells.* J Neuroinflammation, 2012. 9: p. 199.
136. Fuyuki, K., *S100A9/Mrp14 Plays an Important Role in Ab Amyloidosis Enhancement.* Journal of Neurology & Stroke, 2016. 1(2): p. 1.
137. Wang, C., et al., *The role of pro-inflammatory S100A9 in Alzheimer's disease amyloid-neuroinflammatory cascade.* Acta Neuropathol, 2013. 127(4): p. 507-22.
138. Vogl, T., A.L. Gharibyan, and L.A. Morozova-Roche, *Pro-Inflammatory S100A8 and S100A9 Proteins: Self-Assembly into Multifunctional Native and Amyloid Complexes*, in *Int J Mol Sci*. 2012. p. 2893-917.
139. Zhao, L.N., et al., *S100A9 induces aggregation-prone conformation in Abeta peptides: A combined experimental and simulation study.* Scopus, 2013.
140. Zhang, C., et al., *MRP14 (S100A9) protein interacts with Alzheimer beta-amyloid peptide and induces its fibrillization*. PLoS One, 2012. 7(3): p. e32953.
141. Kim, H.J., et al., *S100A9 knockout decreases the memory impairment and neuropathology in crossbreed mice of Tg2576 and S100A9 knockout mice model.* PLoS One, 2014. 9(2): p. e88924.
142. Hawe, A., M. Sutter, and W. Jiskoot, *Extrinsic fluorescent dyes as tools for protein characterization*. Pharm Res, 2008. 25(7): p. 1487-99.
143. LeVine, H., 3rd, *Quantification of beta-sheet amyloid fibril structures with thioflavin T.* Methods Enzymol, 1999. 309: p. 274-84.
144. Minna Groenning, L.O., Marco van de Weert, James M. Flink, and F.S.J. Sven Frokjaer, *Study on the binding of Thioflavin T to β-sheet-rich and non-β-sheet cavities.* 2007. 158(3): p. 358–369.
145. Khurana, R., et al., *Mechanism of thioflavin T binding to amyloid fibrils.* J Struct Biol, 2005. 151(3): p. 229-38.
146. Klingstedt, T., et al., *Synthesis of a library of oligothiophenes and their utilization as fluorescent ligands for spectral assignment of protein aggregates.* Org Biomol Chem, 2011. 9(24): p. 8356-70.
147. Kayed, R., et al., *Common structure of soluble amyloid oligomers implies common mechanism of pathogenesis.* Science, 2003. 300(5618): p. 486-9.
148. Kayed, R., et al., *Fibril specific, conformation dependent antibodies recognize a generic epitope common to amyloid fibrils and fibrillar oligomers that is absent in prefibrillar oligomers.* Mol Neurodegener, 2007. 2: p. 18.
149. Jozef Adamcik, R.M., *Study of amyloid fibrils via atomic force microscopy.* 2012. 17(6): p. 369–376.
150. Wang, C., et al., *The role of pro-inflammatory S100A9 in Alzheimer's disease amyloid-neuroinflammatory cascade.* Acta Neuropathol, 2014. 127(4): p. 507-22.